HEAVY ION BEAM DIAMETER REDUCTION FOR SINGLE EVENT EFFECTS TESTING OF SEMICONDUCTOR DEVICES

A Thesis

by

DYLAN CADE BLEZINGER

Submitted to the Graduate and Professional School of
Texas A&M University
in partial fulfillment of the requirements for the degree of

MASTER OF SCIENCE

Chair of Committee, Rainer Fink
Committee Members, Wayne NP Hung
Jose Silva-Martinez
Head of Department, Reza Langari

December 2021

Major Subject: Engineering

ABSTRACT

Single Event Effects (SEE's) are a common phenomenon in high-altitude semiconductors applications. SEE's are primarily caused by a single ionizing particle, in this case, a heavy-ion striking a single transistor within the Integrated Circuit (IC), causing irregular behavior or device operation. In space environments, high-energy ionizing particles have the potential to jeopardize a mission due to critical computer failure as well as introducing undesirable device operations. SEE's become more common and critical with new semiconductor designs that have a higher transistor density, as the ionizing particle has a greater probability of interacting with a single transistor. Currently, companies such as Texas Instruments Inc. test the effects of high-energy ionized particle strikes on new integrated circuit designs using the Texas A&M Cyclotron Institute K500 beamline.

During the debugging process, specific sections of the DUT must be evaluated with the particle beam, while the remaining portion of the DUT is shielded. The current solution is tedious, inaccurate, and not well understood, resulting in wasted critical reactor time. The current research project describes a system that increases the accuracy of transistor targeting, improves radiation beam diameter reduction, and reduces setup time. The system described was developed in close collaboration with a parallel project providing microscopy and precision alignment.

ACKNOWLEDGEMENTS

I would like to thank my committee chair, Dr. Rainer Fink, who offered valuable guidance and support throughout the span of this research. Additional thanks to Dr. Wayne Hung for providing on campus micromachining resources to produce apertures for test.

Thanks also goes to the Texas Instruments' Space Power Team for providing their expectations and feedback during the initial concept design phase of the project, as well as providing valuable beam time for data collection.

CONTRIBUTORS AND FUNDING SOURCES

Contributors

This work was supervised by a thesis committee consisting of Professor Rainer Fink and Professor Wayne Hung of the Engineering Technology & Industrial Distribution, and Professor Jose Silva-Martinez of the Department of Electrical & Computer Engineering.

The data represented in section 4 was collected with the help of fellow Master of Science in Engineering Technology research student Jackson Wedelich. All other work conducted for the thesis was completed by the student independently.

Funding Sources

Graduate study was supported by a fellowship from Texas A&M University. This research project was partially funded by Texas Instruments Inc..

NOMENCLATURE

DUT	Device Under Test
µm	Micrometer
mm	Millimeter
LET	Linear Energy Transfer
MeV	Mega-electron Volt
MeV/u	Mega-electron Volt per nucleon
eV	Electron volt
V	Volt
SRIM	Stopping and Range of Ions in Matter
in	Inches
mil	Thousands of an Inch
FIB	Focused Ion Beam
SEM	Scanning Electron Microscope
Gaf	Gafchromic Film
LBD	Laser Beam Drilling
kHz	Kilohertz
Nd: YAG	Neodymium-Doped Yttrium Aluminum Garnet
LMIS	Liquid Metal Ion Source

TABLE OF CONTENTS

Page

LIST OF FIGURES

Page

LIST OF TABLES

Page

1. INTRODUCTION

Radiation testing for space application semiconductor devices currently uses a particle accelerator to produce high-energy ionizing particles to interact with the device under test (DUT). Currently, the smallest radiation beam diameter that the Texas A&M Cyclotron Institute K500 beamline can produce (for heavy ions with energy levels in the mega electron-volt (MeV) range) has a beam diameter of approximately one inch. Since the DUT's silicon area is very small (less than one inch) the beam will introduce high-energy particles to the entire DUT at any instant during the test. Therefore, all the active transistors will experience particle interactions simultaneously, making debugging sessions impractical. Texas Instruments Inc. needs to specifically pinpoint very small subsections within the DUT to test for SEE's. Currently, this is done by constructing an aluminum foil tape with a small pinhole which is applied by hand, using a microscope. Although tedious, this will allow the beam to only interact with a small subsection of the chip, possibly even to the single transistor level. Although the manual technique effectively targets a specific section of the chip, it is very time and labor-intensive.

This project aims to decrease the downtime of pinhole construction and alignment time to the targeted semiconductor section. Through the use of precision linear motion stages, micromachining techniques, and pinhole aperture production/procurement methods, test engineers will be able to configure the DUT for a test run in an automated fashion. This will decrease setup time and labor while increasing the effectiveness of test runs and debugging sessions.

1.1 **Review of Relevant Literature**

There are four interrelated topics of research that are being investigated, alpha particle interactions with matter, heavy-ion range tables, unstable radioactive isotope activation for pinhole aperture material selection, and micromachining techniques and capabilities for micrometer hole fabrication.

For alpha particle research, the primary goal is to understand the underlying phenomenon of how alpha particles interact with surrounding matter. The primary mechanism of energy transfer from the alpha particle to matter is Coulombic forces inducing a strong ionization force and electron excitation [1]. Because the structure of an alpha particle is made up of only two protons and two neutrons, it carries a +2-charge inducing a strong ionization force that can attract any electrons that are relatively near the charged particle trajectory [2]. With each ionizing event, the alpha particle will transfer some of its kinetic energy to the electron due to the electron binding energy, and therefore not necessarily only losing kinetic energy due to inelastic collisions. Electron excitation occurs when the strong ionization force does not exceed the electron binding force of the electron, therefore putting the electron into a higher energy state [3]. This suggests that in its initial trajectory, the dominant force that the alpha particle has on the surrounding electrons is primarily the ionization force. As the particle gradually loses energy, electron excitation becomes more dominant, until the Bragg peak. When the electron comes back down into a balanced low energy state, it will release this energy in the form of heat[4].

The purpose of researching unstable isotopes is to identify materials that have a low half-live. The initial material considered for beam diameter reduction aperture is Series 1000 Aluminum foil sheets, which consist of 99% Aluminum 27 (^{27}Al). ^{27}Al is the only stable Aluminum isotope that is readily abundant on earth. An isotope becomes unstable and undergoes transmutation only when there is a force among the particles in the nucleus that makes it unbalanced. This form of excess internal energy typically comes in the form of a neutron being ejected or added to the nucleus. To expel this excess energy, the nucleus will emit some type of particle or form of energy. This is the basic formulation of radiation. In this case, unstable isotope ^{26}Al is created when a single neutron is ejected from the nucleus, causing an imbalance of internal energy. Throughout its half-life (716,000 years), the unstable isotope will transmutate into Magnesium 26 (^{26}Mg) [5]. This would mean that the alpha particle would need to directly collide with the Aluminum nucleus with at least 8.3 MeV of energy to have the possibility of dislodging a neutron from the nucleus. This gives cause for concern for the potential to create the ^{26}Al radioactive isotope and having to deal with its relatively long half-life. For this, a thorough understanding of the expected collisions needs to be addressed.

Three types of collisions will occur during beam test runs: (I) inelastic electron collisions, (II) inelastic nucleus collisions, (III) elastic scattering with a nucleus. Because these are high-energy particles, inelastic electron collisions will be the dominant mechanism between particles, which will enable the strong ionization force and electron excitation to take place. In inelastic nucleus collisions, the alpha particle will deflect its

trajectory from the aluminum nucleus, regardless of isotope form, primarily due to both nuclei having a net positive charge and repelling force applied. Due to this deflection, some alpha particles may release energy in the form of electromagnetic radiation, known as bremsstrahlung radiation [6]. There is also a case where the alpha particle can deflect from the aluminum nucleus without releasing any forms of energy, known as elastic scattering with a nucleus. Elastic scattering mainly only occurs with low-energy particles. Because the Aluminum nucleus will not experience direct collisions with a high-energy alpha particle, it is improbable that the nucleus will experience a force greater than the binding force resulting in ^{26}Al.

For micromachining techniques for aperture production, there are three notable and readily available techniques: (I) Focused Ion Beam (FIB), (II) Laser Drilling, (III) Photochemical etching.

Two mechanisms categorize these techniques: (I) Bulk micromachining and (II) Surface micromachining. Bulk micromachining focuses on forming structures by etching a selective position inside the substrate, while surface micromachining forms structures on top of the substrate [7]. For aperture fabrication, the bulk micromachining mechanism will be used.

Focused Ion Beam uses a beam of positively charged ions that can directly mill the desired feature in the form of bombardment effectively sputtering atoms from the substrate.

Laser drilling uses a highly intensive light beam that either exceeds the material's ablation threshold or heat the material thermally to etch the feature into the substrate [8].

The ablation threshold of the film is defined as the critical fluence (optical energy per area per pulse) which results in material removal within the irradiated spot area [9]. Depending on the wavelength and optical configuration of the instrument, micrometer-scale features can be etched into the substrate.

Photochemical etching, using lithography technique, can produce nanometer range features. A photo resistive film is first spin-coated on the surface of the substrate, where then UV light containing the pattern of the desired feature erodes the film and exposes the material to be chemically etched [10]. This technique can quickly and produce nanometer range features at a relatively low fabrication price while retaining repeatability.

2. BACKGROUND

2.1 Alpha Particle Interactions with Matter

Because the beam diameter reduction aperture primarily operates in a radioactive environment, there is a need to understand the fundamentals of how alpha particles interact with surrounding matter. An alpha particle consists of two protons and two neutrons with no surrounding planetary electrons. The particle is sourced from an unstable isotope undergoing alpha decay. Currently, Texas Instruments uses four sources to produce a heavy-ion alpha particle for test. This includes Holmium, Praseodymium, Silver, and Krypton. Heavy Ions are defined as particles that carry one or more units of charge. Because the particle has no planetary electrons, it carries a +2 charge which will be the primary mechanism for surrounding matter interactions. This introduces three primary phenomena that describe how the particle interacts with surrounding matter. This includes inelastic electron collisions, inelastic nucleus collisions, and elastic nucleus scattering.

Inelastic electron collisions introduce strong coulombic forces and electron excitation. Due to the +2 charge of the particle, the strong coulombic force will eject any valence electrons and ionize atoms near the particle track which mainly consists of air gas, aperture material, and silicon material making up the DUT. There is also a similar case for atoms that are relatively far away from the particle track. For this, electron excitation is the primary mechanism where the particle transfers energy to an electron and puts it into an excited state. The electron releases this energy in the form of heat to

return to a stable state. In both cases, kinetic energy is not conserved and is transformed to heat.

Inelastic nucleus collisions occur when the positively charged particle directly collides with a net positive charged ionized particle or atom. In this scenario, the like charges repel and divert the alpha particle from its original trajectory. This encourages diffusion that will be introduced in further detail in section 4.3. Because this is an inelastic collision, the particle energy is transformed to either heat or electromagnetic radiation also known as bremsstrahlung radiation.

Finally, in nucleus scattering, the alpha particle directly collides with low-energy nuclei that also have a net neutral charge. Because no charges are enacting upon one another, the alpha particle will divert from its original trajectory after collision, encouraging diffusion. It is important to note that although the overall system kinetic energy is conserved, the alpha particle will transfer some of its energy onto the stationary particle, and no amount of energy is transformed to heat. Due to this direct physical collision, there is a potential that the target material can become unstable and undergo decay also known as radioactivity.

An isotope becomes unstable and undergoes transmutation only when there is a force among the particles in the nucleus that makes it unbalanced. This form of excess internal energy typically comes in the form of a neutron being ejected or added to the nucleus. To expel this excess energy, the nucleus must emit some type of particle or form of energy, thus the basic formulation of radiation. Transmutation is the process of an original isotope transforming into a new chemical element. For instance, Aluminum

27 (^{27}Al) will transmutate into Magnesium 26 (^{26}Mg) when it becomes unstable. An important characteristic that must be addressed is half-life. Half-life is defined as the amount of time required for an unstable isotope to reach half of its initial radioactivity. In the case that our aperture material becomes radioactive, the half-life time must be acceptable for the system to be safely removed from the Cyclotron facility.

It is important to understand and calculate how much energy a particle is transferring into the surrounding matter. Linear energy transfer (LET) is the rate of energy an ionized particle transfers to matter per linear unit distance. This parameter directly represents the range of an ion that travels through the material and enables researchers to calculate and analyze ion range tables that will help in material selection. Two characteristics affect ion penetration range: material density and initial particle energy. With a high material density and low particle energy, the energy transfer rate will be relatively high resulting in lower penetration. If a low-density material is a target for a high-energy particle, the LET value will be low and high penetration will result. For this aperture application, a high LET value is desired. Because the initial particle energy is constant, highly dense material is needed to produce a high LET value.

Opposite from its name, linear energy transfer, the amount of energy transferred per distance, is in fact not linear. As the kinetic energy and speed of the particle decrease, there is more time for the particle to expend its energy relative to its previous position. Therefore, the magnitude of overall energy transferred increases exponentially as the particle travels throughout its track. This is seen in the Bragg curve shown in figure 2.1. There is a unique point on the curve that describes how the particle reacts as it

approaches near-zero overall kinetic energy, also known as the Bragg peak. Directly after this point, the particle loses all kinetic energy, and the alpha particle acquires two electrons and transforms into helium gas.

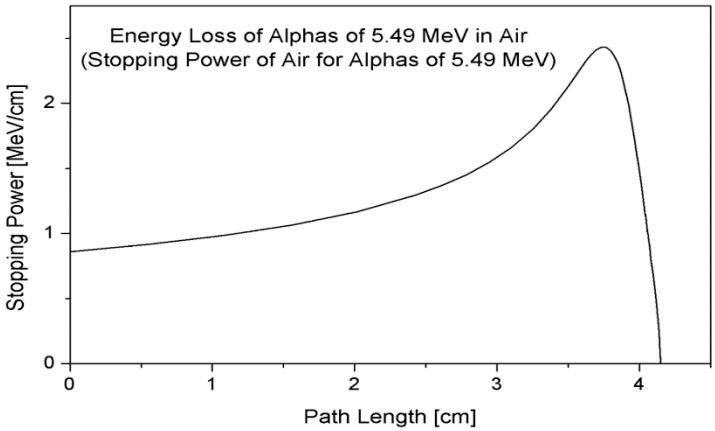

Figure 2.1: Bragg Curve

With a large approximate mass of 6.642x10-4 grams, the particle has the potential to carry large kinetic energy. In particle accelerators, the standard unit electron volt (eV) is used to describe this amount of energy. One eV is defined as the amount of energy a particle gains when it crosses an electrical field of 1V. In this case, Texas Instruments Inc. is conducting radiation testing with particle energy of no less than 15 MeV/u and some tests require 24.8 MeV/u beams.

2.2 Ion Range Tables and Material Selection

As discussed previously, knowing the range that the particle will penetrate the aperture material is crucial information for material section. For the aperture material to

function as desired, the material should absorb all of the particle energy and not let any through. Only particles going through the aperture hole should impact the semiconductor material being irradiated. Section 2.2 will describe the basic mathematical formula and three software packages used to identify ion range, given ion type, energy, and material density.

The basic mathematical formula for ion range is shown in equation 2.1. This formula takes inputs for the ion energy (E), atomic mass (A), and density (ρ) of aperture target material and returns the range in milligram per square centimeter (R_{mg/cm^2}).

$$R_{mg/cm^2}=0.173E^{3/2}A^{1/3}$$

To transform the range in units of density to microns (μm), the output from the original range formula is divided by the density of the aperture material (ρ), and the quotient is multiplied by 10,000 as shown in equation 2.2.

$$R_{cm} = (R_{mg/cm^2}/ \rho)*10000$$

For ion range calculations, Aluminum will be used as a baseline aperture material to calculate the penetration range of a 15 MeV/u ion. With a density of 2.7g/cm^3, a 15 MeV/u ion has a range of 111.5636μm. This value will be used to compare output range tables from the software packages.

The first software package used is Stopping and Range of Ions in Matter (SRIM). This software outputs a range of ion penetration values given ion type, input energy range, and material density. A limitation of SRIM is that it only accounts for a single material layer and no air gaps, which will be needed to accurately simulate the ion in the expected Cyclotron environment. Using the same input parameters as with the mathematical formula, the penetration range in Aluminum is 132.57μm. We can see that the output of SRIM is approximately 21μm higher than the calculated value. This difference primarily comes from the ion type input of the equation.

The second software package used to determine material thickness is Seuss control software. This software is the primary control software for the Texas A&M Cyclotron. The Cyclotron package offers control of real-life hardware including beam degrader settings, DUT positioning system control, beam characteristics, and beam degrader tuning. In contrast to the SRIM software package, the Seuss software considers the layer setting that is currently selected. Here the layer settings allow the user to define their test setup for the software to calculate DUT penetration while considering current beam settings, air gaps, and other penetrated materials. Seuss reflects an accurate aperture material thickness value needed to stop the undesired sections of the beam and result in 0μm of DUT penetration. The required Aluminum thickness to stop the beam is reported as 132.7μm. The difference of output between SRIM and Seuss software packages is minimal, therefore validating both software packages.

The final software package used to visualize beam diffusion is TRIM. This software package simulates the spread of the beam after penetrating a theoretical

flat sheet of Aluminum with a given thickness. It is important to note that this software is only used to visualize the beam diffusion, and measurements are not available in this software. The simulation output with Aluminum material and a 7mm air gap is shown in figure 2.2.

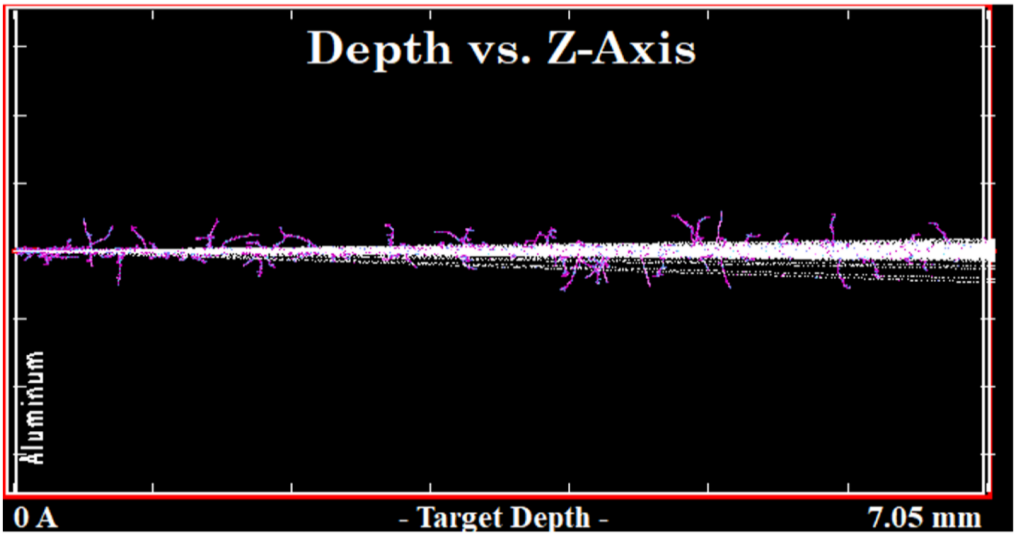

Figure 2.2: SRIM Simulation Output

2.3 Micromachining Techniques

To produce a range of micron-level diameter pinholes, an in-depth explanation of micromachining techniques is needed. There are two main categories of micromachining: Surface Building and Bulk Etching. Surface building is an additive method that builds the features on top of the surface of the substrate, while bulk etches the future into the substrate. Because we are mainly focused on etching a round hole through the substrate, this paper will focus and describe bulk etching techniques.

There are two subcategories of bulk etch: Wet and dry etching. Wet etching uses a chemical etchant and a photomask to specifically outline the feature for the chemical to etch the feature. With dry etching, the feature is formed either through the bombardment of high-energy particles or using reactive vapor etchants in a plasma environment.

A common instrument that is categorized under bombardment of high-energy particles is the Focused Ion Beam (FIB). FIB uses a beam of positively charged ions that can directly mill the desired feature in the form of bombardment effectively sputtering atoms from the substrate. By precisely controlling the energy and intensity of the ion beam, a highly detailed and precise feature in the nanometer range can be etched into the substrate. A typical ion source for FIB instruments is Xeon (Xe+). Xe+ is a Liquid Metal Ion Source (LMIS) that has a low melting point at room temperature. The LMIS is melted in a reservoir that is connected to a tungsten tip that has a high electric field applied to it. When heated, the metallic liquid conforms around the tip and the strong electrical field directs the ions to the substrate for machining.

High-powered lasers fall under the category of reactive vapor etchants in a plasma environment. Another common name this is referred to is Laser Beam Drilling (LBD). The primary mechanism for etching is the intensity of the focused light beam that rapidly heats the material. Material removal methods can be different as some systems can vaporize the material, while other systems use an assist gas to blow away molten material from the workspace. Multiple types of lasers are used to cut submicron features into a variety of substrates, ranging from glass, metals, and ceramics. This

document will describe two laser types identified for use in this project: Picosecond Pulsed Laser and Neodymium-Doped Yttrium Aluminum Garnet (Nd: YAG) Laser.

The ultra-short picosecond pulsed lasers employ a focused light beam with a set intensity, that is pulsed at a frequency typically in the kHz range, to etch a feature into a substrate. The proper term for material removal using laser-based machining systems is referred to as ablation. With each pulse, high energy (typically 10W) is transferred into the material, heating and ablating the substrate multiple times, until the desired feature is formed. These lasers are particularly effective at drilling small holes with a diameter of less than 100µm in substrate materials less than 500µm thick. Ultra-short laser-based systems show clear advantages concerning machine quality, heat-affected zone, and minimal debris over multiple publications[11]. In these systems, a galvo scan head is used to direct the light beam from the source to different sections of the substrate. A helical drilling pattern is shown to produce the best results for edge and sidewall quality of the hole.

Nd: YAG Laser based systems uses a highly focused light beam to heat the substrate. Some systems can be either pulsed or continuous. Other than the light beam being sourced from a different source, the primary difference from picosecond pulsed lasers is that YAG laser systems apply more aggressive energy onto the substrate, creating a pool of molten material where a continuous flow assist gas removes the molten metal from the work area. Due to the molten metal being blown away from the work area, a splatter formation forms around the hole and requires additional processing to remove this slag. Slag is a disadvantage when using Aluminum substrates because re-

solidified material can build up along the diameter of the inlet hole. Numerous process and performance parameters are used to fine-tune the laser to yield better results and in reducing splatter formations and re-solidified material buildups.

3. METHODS

3.1 Material Selection

Material selection was based on two parameters: radioactive isotope half-life and material thickness. Three materials were identified to test: Aluminum, Silicon, and Copper. Section 3.1 will identify the advantages and disadvantages of each material.

Aluminum was first chosen primarily to serve as a baseline test to validate the current methods of beam diameter reduction from Texas Instruments test engineers. For procurement purposes, Series 1000 99% pure Aluminum is relatively available in foil form at a low price. Unfortunately, the major disadvantage of this material outweighs the advantages. Due to the low melting point of Aluminum, laser micromachining is very difficult as there is a high risk of degrading edge quality, directly affecting the quality of the reduced diameter beam. Also, during FIB machining sessions, it was found that the time to form a complete 25µm diameter hole through Aluminum was impractical, estimated to be greater than 100 hours. This time would only increase when attempting features larger than 25µm. Furthermore, in the case that the Aluminum did become radioactive, the half-live is estimated to be 716,000 years. Due to these disadvantages, Aluminum was determined to be a non-ideal choice for aperture material.

Silicon was primarily chosen due to its low FIB machining time. From FIB machining sessions, it took approximately 15 minutes to create a 100µm diameter feature at 60µm depth. Additionally, the half-life of radioactive ^{28}Si is less than five seconds, which is highly desirable. The overall properties of Silicon make this material

ideal for aperture material. The main issue for Silicon is the unavailability to procure Silicon wafers less than 300µm thick. This thickness furthermore reveals limitations of FIB ability to create high-quality micro-level diameter holes. These limitations will be covered in section 3.3.

The final material identified for aperture material was Copper. This material is commonly used as the base material for high power apertures, is easily obtainable in foil form, and has an acceptable half-life of less than ten minutes. Because Copper has a higher melting temperature compared to Aluminum, there will be less solidified material on the diameter of the hole, resulting in a cleaner cut. The only disadvantage that Copper has, is that it naturally oxidizes over time, leading to a green tarnished surface that could potentially comprise the material's ability to produce a uniform recued diameter beam.

3.2 Thickness Requirements

Now that the three materials have been identified for test, both SRIM and Seuss software packages will be used to determine the minimum thickness. The inputs for these calculations are the same as described in section 2.2. That is a Holmium heavy-ion beam with an energy of 15 MeV/u. Table 3.1 lists the required minimum thickness to fully stop the beam for each material.

Aluminum	Silicon	Copper
132.57µm	150.64µm	49.6µm

Table 3.1: Required Minimum Thickness

3.3 Micro Machining Processes and Outcomes

There were three processes used to produce a micron-level hole into the selected materials. Manual drill bit and razor blade techniques done by hand to replicate current pinhole production; FIB FERA Xeon source Instrument resourced from the on-campus Material Characterization Facility (MCF); and Ytterbium Fiber Laser instrument resourced from the HAAS Technical Education Center Facility on-campus.

Using the Aluminum material as the substrate, the drill bit and razor blade are relatively simple production methods as they do not require special and complex instruments. The smallest drill bit that was sourced had a diameter of 320µm. This makes the drill bit highly prone to breaking regardless of the carbide alloy that it is constructed from. The razor blade is easier to handle, keeping in mind of the sharp edge, but it is incapable of making repeatable diameters smaller than 700µm. The disadvantage of these techniques is that hole placement by hand is extremely inconsistent in relation to drilling the hole in the same relative location on the Aluminum foil substrate. Additionally using the razor blade, the user has limited control over the final diameter of the hole and quality of the hole leading to major edge defects. The results of these techniques will be covered in more detail in section 4.1.

The FIB was shown to be capable of producing high-quality circular features but is limited to low thickness materials less than 100µm. Because we are using an on-campus academic resource, the instrument is only available for four hours per session. During the first hour, the instrument requires a relatively high and stable vacuum to

function appropriately, meaning there are roughly three hours of machining time per session. As mentioned previously in section 3.1, the FIB is effective in creating high-quality sub-micron features in Silicon, but past 60µm in hole depth more issues of sputter funneling, and beam convergence started to occur. Figures 3.1 and 3.2 will be used to visualize the beginning stages of these affects. These figures show a SEM image of a 100µm diameter hole being attempted in Aluminum substrate.

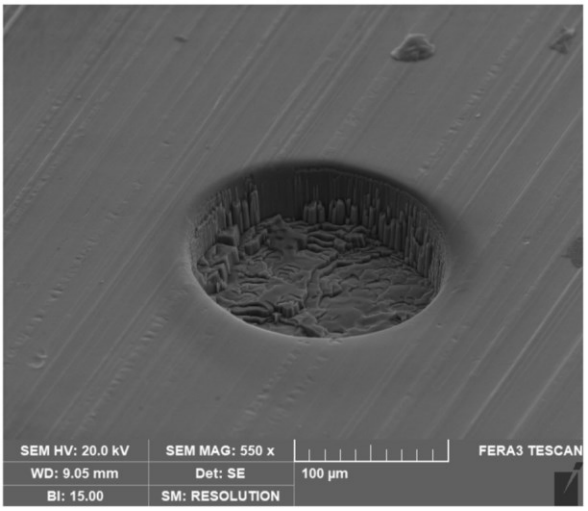

Figure 3.1: 40µm Depth, 4 Hours

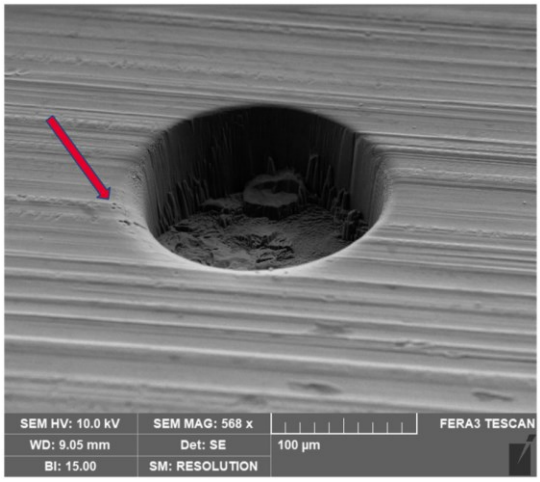

Figure 3.2: 60µm Depth, 7 Hours

In Figure 3.1, we see the feature at 40µm of depth after four hours of machining. The quality of the hole is acceptable as there are minimal edge defects. Figure 3.2 shows the same feature at 60µm of depth after 7 hours. Indicated by the red arrow, we observed a larger edge radius starting to form only on one side of the feature. The same effect was observed when attempting to etch a 25µm diameter hole in Silicon. This larger radius is due to sputter funneling. As discussed earlier, the sputtering mechanism dislodges atoms from the crystal structure to form the feature. As the focused ion beam propagates further into the material, the atoms are essentially getting trapped between the beam and the sidewalls of the substrate. This leads to the sputtered atoms jetting upward along the sidewall to escape, etching material along the way. This forms a channel for the sputtered atoms to jet through, leading to a non-circular feature.

Another issue that was observed with FIB after a certain thickness, is that the sidewalls started to taper inward toward the center of the feature. This phenomenon can be better understood in Figure 3.3. This illustration is the theoretical cross-section showing how the beam converges to a focal point within the thickness of the material.

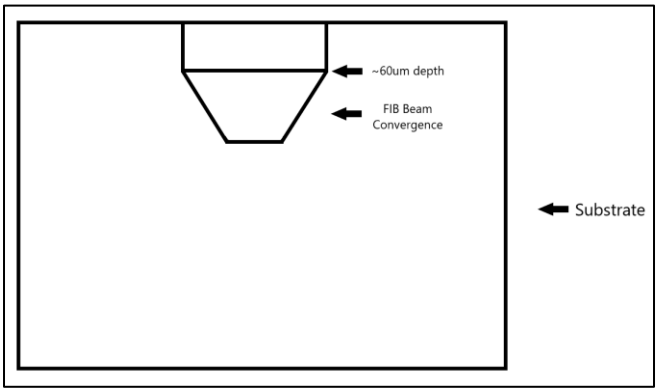

Figure 3.3: Illustration of Beam Convergence

When a program is made to etch a 25µm hole through the substrate, the instrument will adjust the beam to have a 25µm diameter only on the surface of the substrate. The depth of the feature is not considered; therefore, the beam will converge to the focal point within the material.

3.4 Project Convergence and Collaboration

To ensure that the two projects integrated seamlessly, there had to be close collaborations with Jackson Wedelich, who was the researcher and designer for the alignment and microcopy portion of this system. Some design constraints were created to ensure that the microscope would not mechanically interfere with the microscope 100x objective. This objective had the smallest working distance of 7mm. Additionally, the DUT PCB boards typically have other passive electrical components that can have a height of 3mm. Overall, the total thickness of the pinhole aperture support frame had to be no more than 4mm thick. Because the pinhole positioning between the DUT and the microscope was critical, the PCB Board mounting bracket, Pinhole-PCB Board group

main support brackets became part of this thesis. To ensure that the space between the DUT and the pinhole aperture was minimized, a manual adjustment with micrometer movement capabilities was installed. The manual adjustment also gives the system the ability to test a wide variety of DUT's regardless of their height from the PCB board. Because the microscope had to be moved in and out of the beamline to align the pinhole to the desired transistor target, the linear actuator rail holding the microscope makes it were the main support bracket for the PCB board mount and the pinhole support frame must reach over the microscope rail to meet the 40mm air gap requirement. To minimize the amount of reach, a main Solidworks model was created to incorporate both the mechanical design mentioned here but also that of Jackson Wedelich. This ensured that both MSET designs integrate mechanically and meet the overall system requirements without interference issues.

Jackson and I collaborated on other portions of the system including LabView/Teensy communication protocol and message definition, stepper motor driver electronics, and PCB board design. These are reported in a separate thesis by Jackson Wedelich.

4. RESULTS

There were three tests performed in total: measuring physical pinhole diameter and quality, measuring dosed diameter, and measuring total reduced beam diffusion. For physical measurement of the pinholes, the microscope EP-View Software was used. This software features an intuitive graphical user interface (GUI) that has calibrated measurements and was used to measure pinhole diameter and to characterize the quality of the hole. For the remaining two tests, a Gafchromic (Gaf) radioactive film was used to record the results of the reduced diameter beam. Whenever the surface of the film encounters a high-energy ion, the color of the film transforms from yellow to gray. The overall darkness of the grey depends on the amount of dose that it received. If a higher dose is received, the grey spot will become darker.

The test setup for the dose diameter tests consisted of a 3D printed bracket holding the pinhole aperture stationary and a Gaf film mount holding the film at two different distances away from the surface of the pinhole. For dosed diameter test, the Gaf film was mounted 2mm away from the pinhole. For the beam diffusion test, two beam runs were conducted using the same pinhole. For the first run, a single section of Gaf film was set 2mm away. The second run used a new section of the Gaf film set at 29mm away.

To measure the diameter of the grey spot on the film, ImageJ analysis software was used to create surface gray-value vs distance plots in a horizontal and vertical slice. An example of a gray-value vs distance plot is shown in figure 4.1.

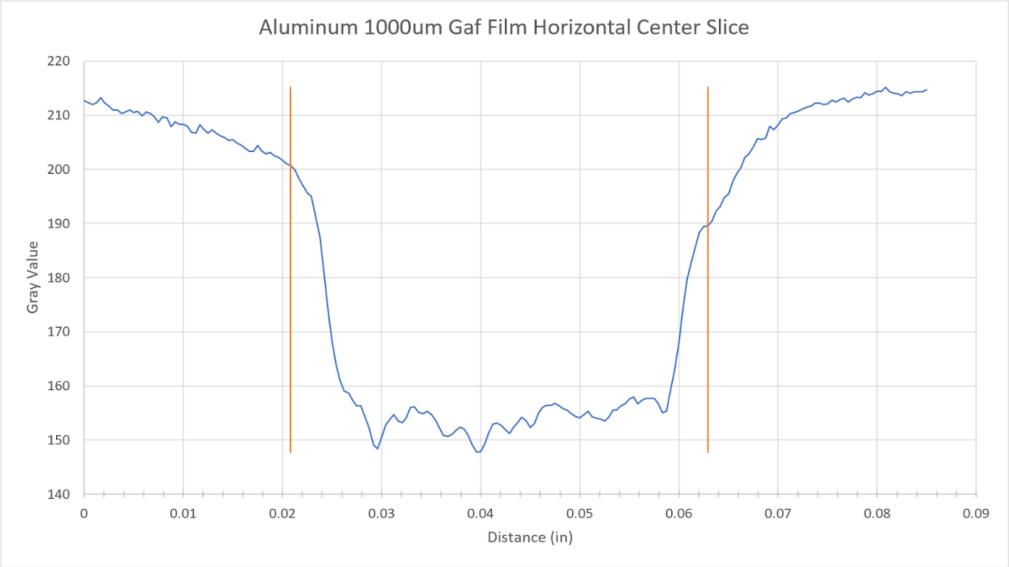

Figure 4.1: Example Grey Value vs Distance Plot

In Figure 4.1, a higher grey-value in the Y-axis is inverse of what is found on the actual film. A darker gray spot on the film correlates to a lower gray value. The general outline of the dose diameter can be visualized, but from this plot it is hard to dictate the starting and ending points of the dosed diameter. By taking the derivative of the raw data, it is clearly defined where the beginning and end of the dosed diameter are located. An example plot of gray derivative values vs distance is shown in figure 4.2.

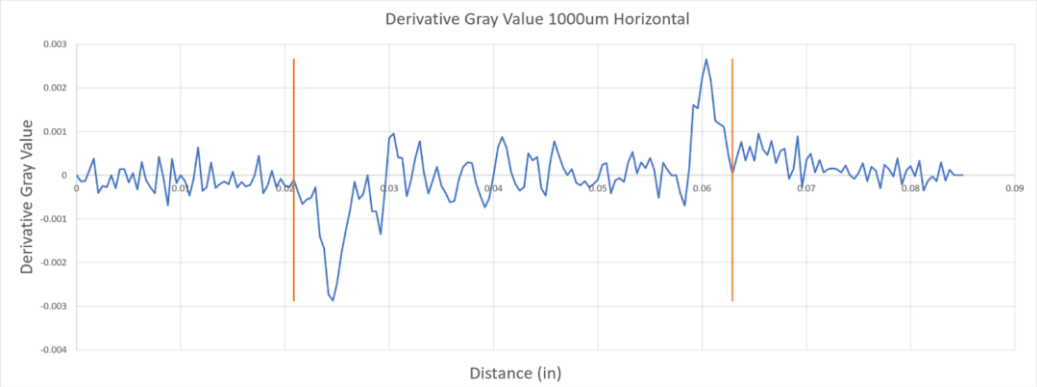

Figure 4.2: Derivative Gray Value vs Distance Plot

In Figure 4.2, the spikes represent the rapid change in slope. Here I created two rules for determining starting and stopping locations. The starting point is located at the last data point to touch the zero line before the first spike occurs. The ending point is located at the first data point to touch the zero line after the second spike occurs. The same analysis was applied for determining beam diffusion.

4.1 Physical Pinhole Diameter

All the produced pinholes were measured and analyzed. This includes all of the procured Lenox Laser Copper high power apertures (Figures 4.3 – 4.9), both Aluminum fiber laser pinholes (Figures 4.10 and 4.11), and both Aluminum hand-produced pinholes (Figures 4.12 and 4.13).

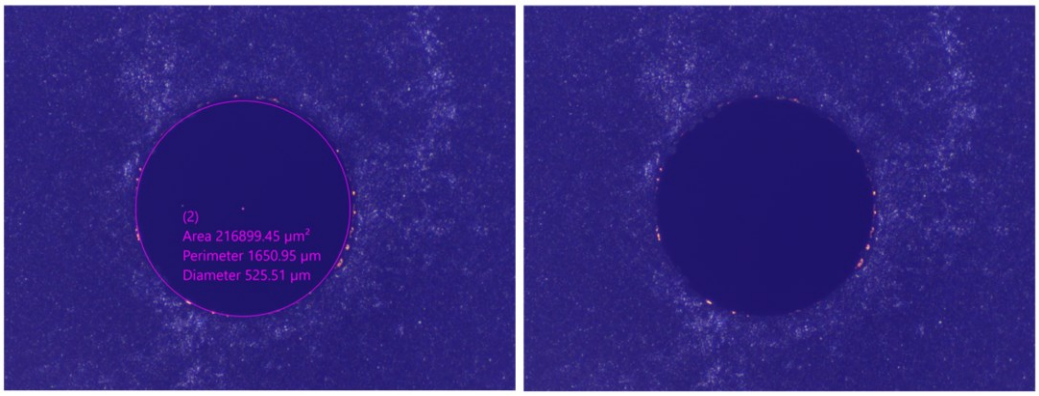

Figure 4.3: Lenox Laser 500µm Diameter Aperture

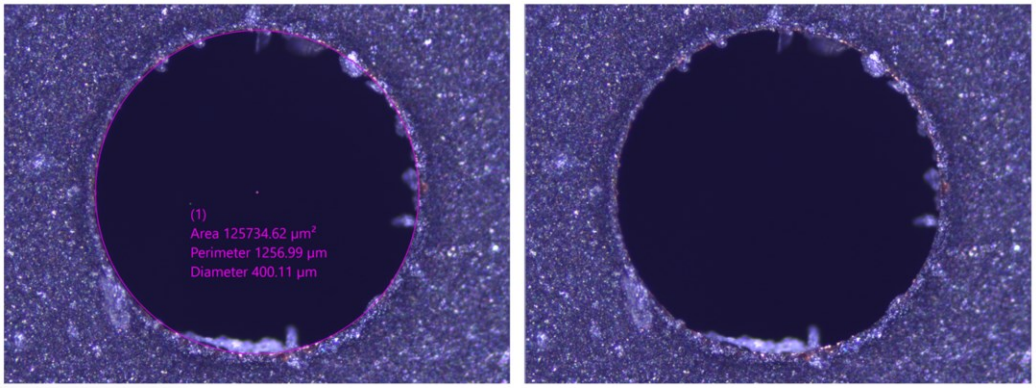

Figure 4.4: Lenox Laser 400µm Diameter Aperture

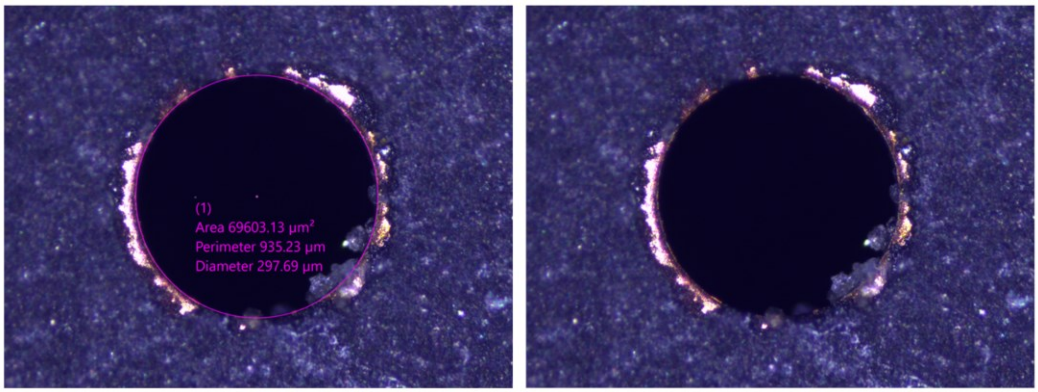

Figure 4.5: Lenox Laser 300µm Diameter Aperture

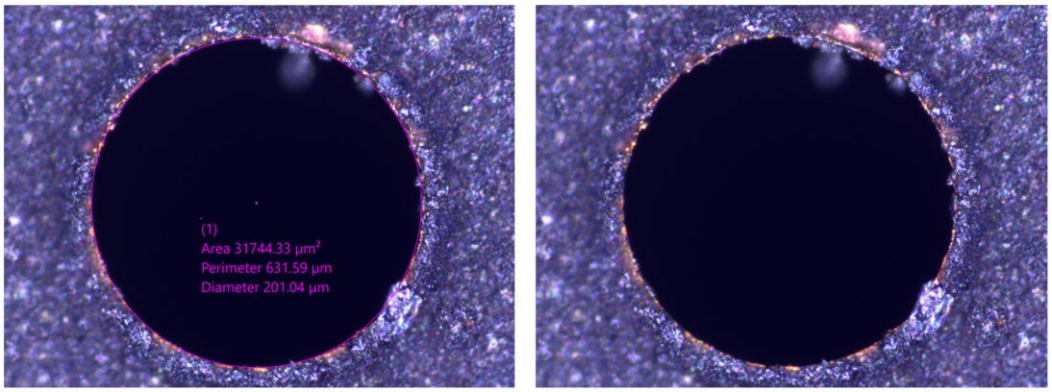

Figure 4.6: Lenox Laser 200µm Diameter Aperture

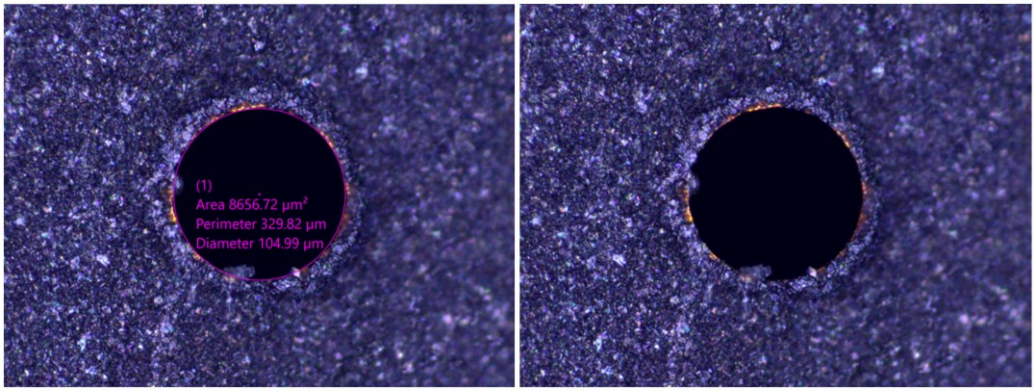

Figure 4.7: Lenox Laser 100µm Diameter Aperture

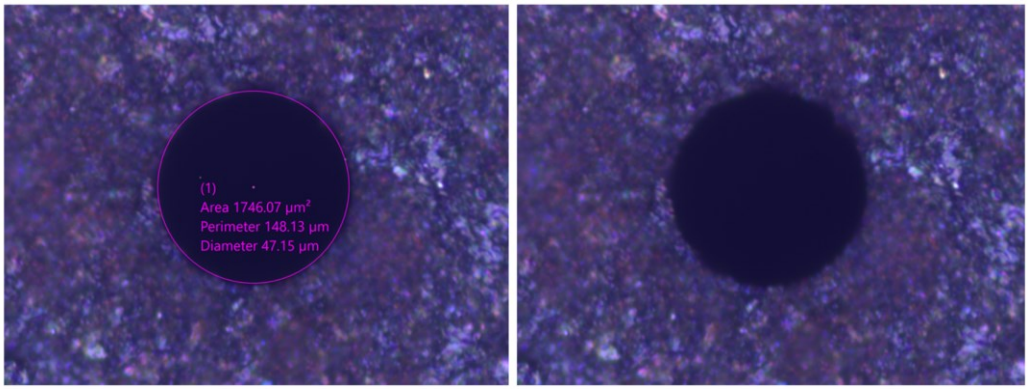

Figure 4.8: Lenox Laser 50µm Diameter Aperture

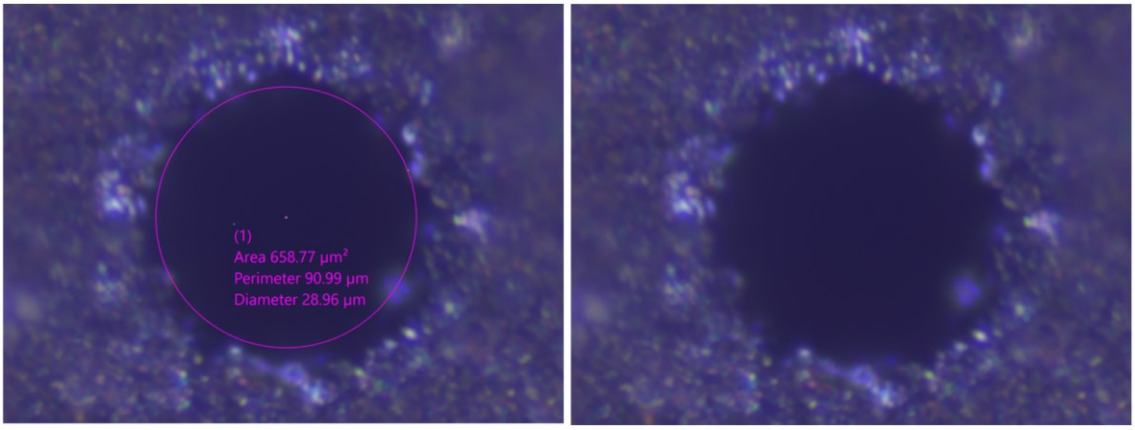

Figure 4.9: Lenox Laser 25µm Diameter Aperture

Each of the Lenox Laser Copper apertures was ordered with a black coating to minimize reflections while viewing the pinhole through the microscope. Figure 4.5 shows some of the black coating flaking off, exposing the Copper base material underneath. Some of the flaking is seen to obstruct the middle of the pinhole, this is not a concern as the heavy ion beam will fully penetrate through the coating without affecting the quality of the reduced diameter beam. Figure 4.9 also shows the blackened coating overlapping the edge of the 25µm diameter pinhole. The assumption can be taken as with the 300µm diameter pinhole, where the overlap will not affect reduced beam diameter quality. Overall, the edge quality of the holes is high and is held as the golden standard with minimum error in true diameter.

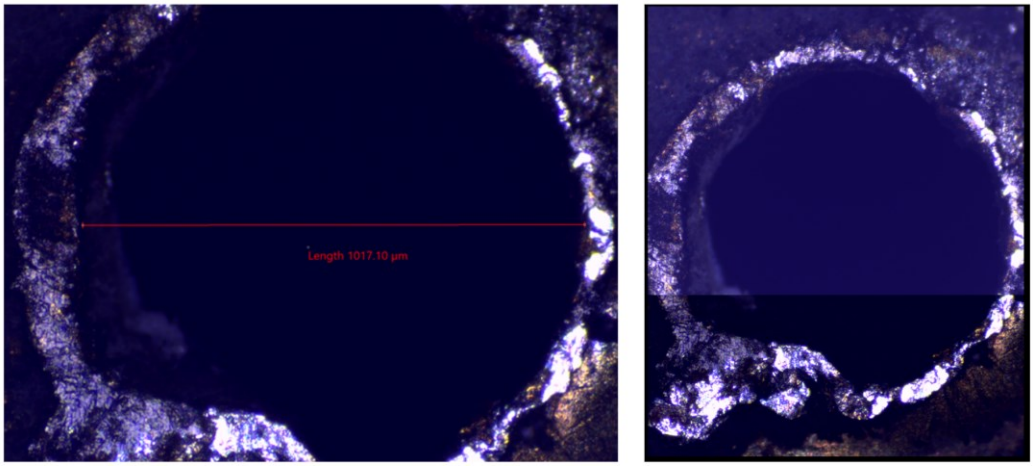

Figure 4.10: Fiber Laser 1000µm Diameter Aluminum

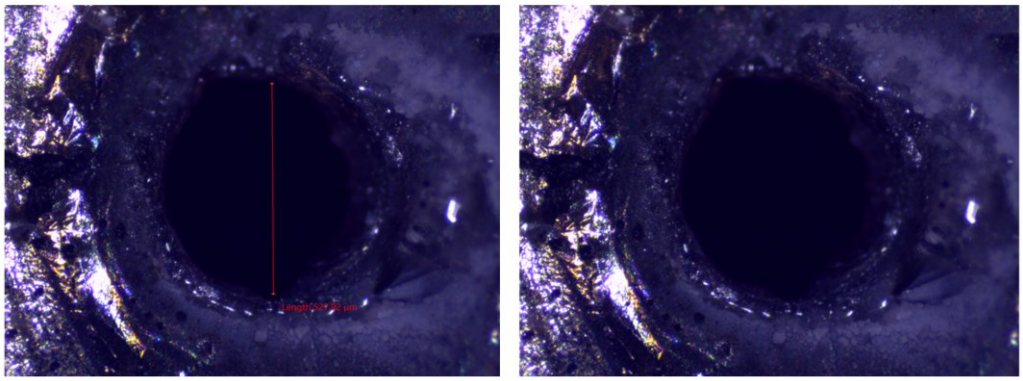

Figure 4.11: Fiber Laser 500µm Diameter Aluminum

In the initial test run, Ytterbium Fiber Laser Aluminum apertures are seen to have large defects, as shown in Figure 4.10. The overall diameter was estimated to be 1017.1µm, excluding the large defect toward to bottom left of the hole. These figures also show that some sections of the sidewall are not perpendicular to the surface. Both major defects will lead to a non-circular dose diameter shown in section 4.2.

The 500µm diameter hole seen in Figure 4.11 is a second attempt with adjusted parameters to produce a higher quality hole. The overall diameter, estimated to be

527.92µm, shows no major defects and is relatively circular. The main defect in this test sample is the right sidewall. Due to the low melting temperatures of Aluminum, the sidewall is shown to be melted rather than a clean cut, negatively affecting the dose diameter.

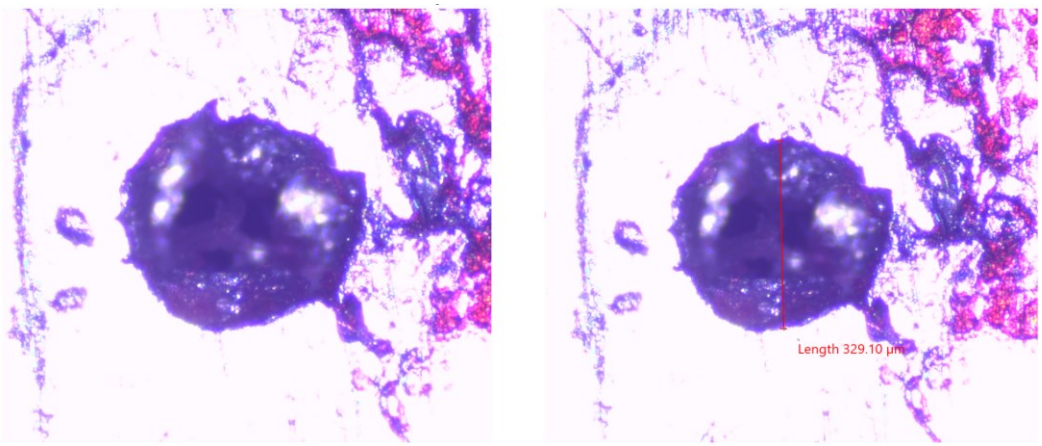

Figure 4.12: 320µm Diameter Drill Bit Aperture

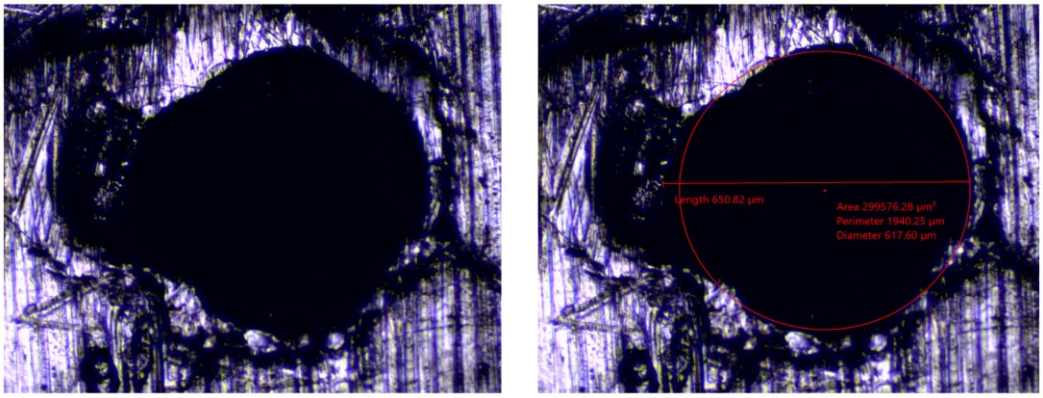

Figure 4.13: 700µm Razor Blade Aperture

As stated before, the main purpose for hand-producing Aluminum apertures is to mimic pinhole production practices currently used by Texas Instruments and to serve as a baseline test. In Figure 4.12 the 320µm diameter drill bit was used to produce the hole.

It is difficult to measure the exact diameter of the hole, but it was estimated to be 329.1µm. As shown here, there is a significant amount of edge defects and burrs. The 700µm diameter razor blade test produced better results. The edge is mostly circular, with exception of the large burr defect on the left side of the edge. Regardless of the quality of the hole produced, it is extremely difficult to precisely place the hole in a specific section of the Aluminum foil by hand, leading to difficulties aligning the hole to the desired transistor group using the precision alignment system.

4.2 Gaf Film Dosed Diameter Measurement

The purpose of the Gaf film dosed diameter test was to measure the irradiated area with a DUT that is placed 2mm away from the aperture. The apertures that were used are as follows: Lenox Laser 500µm Copper diameter, fiber laser Aluminum apertures, and the razor blade 700µm Aluminum aperture. Each test will show the Gaf film image scan, raw data output, and derivate data transformation for the horizontal and vertical respectively.

The first analysis is the Lenox Laser 500µm Copper Aperture. Figure 4.14 shows the Gaf film image scan, and figures 4.15 – 4.18 show the raw data and derivative data for horizontal and vertical slices respectively.

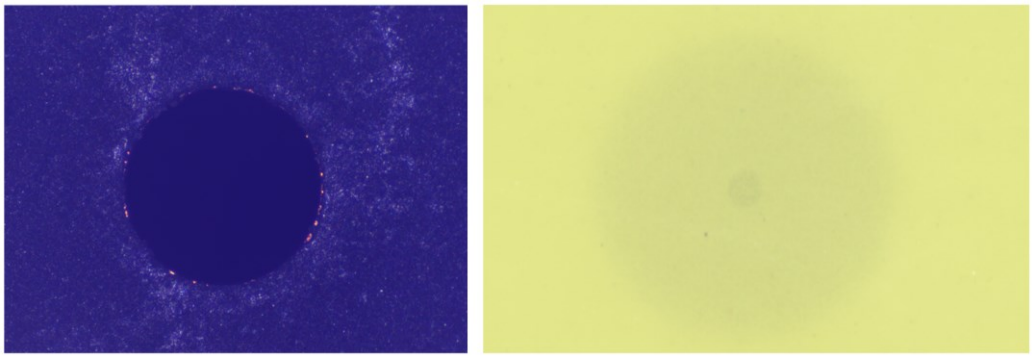

Figure 4.14: Copper 500µm Gaf Film Image Scan

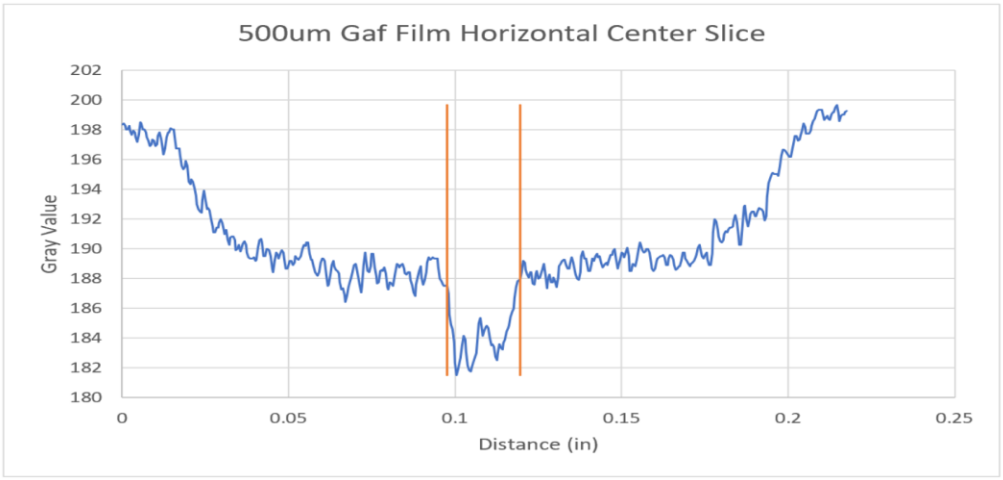

Figure 4.15: Copper 500µm Raw Data Horizontal Slice

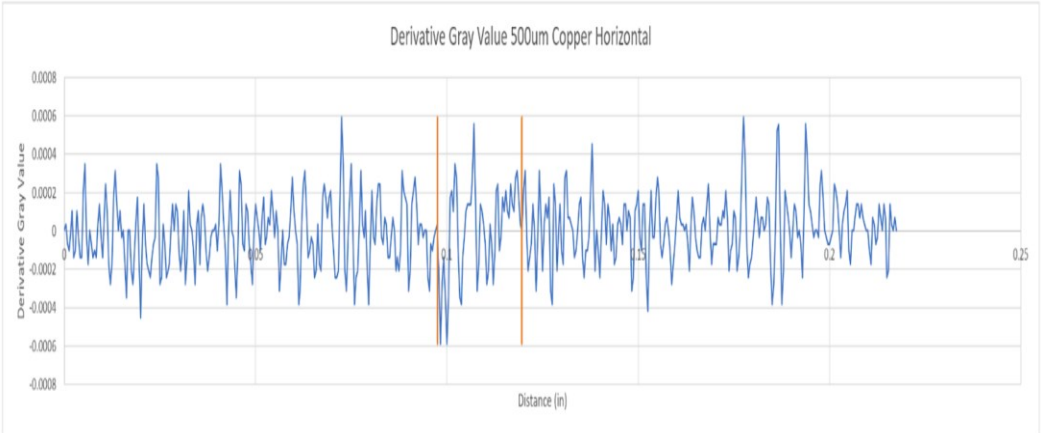

Figure 4.16: Copper 500µm Derivative Data Horizontal Slice

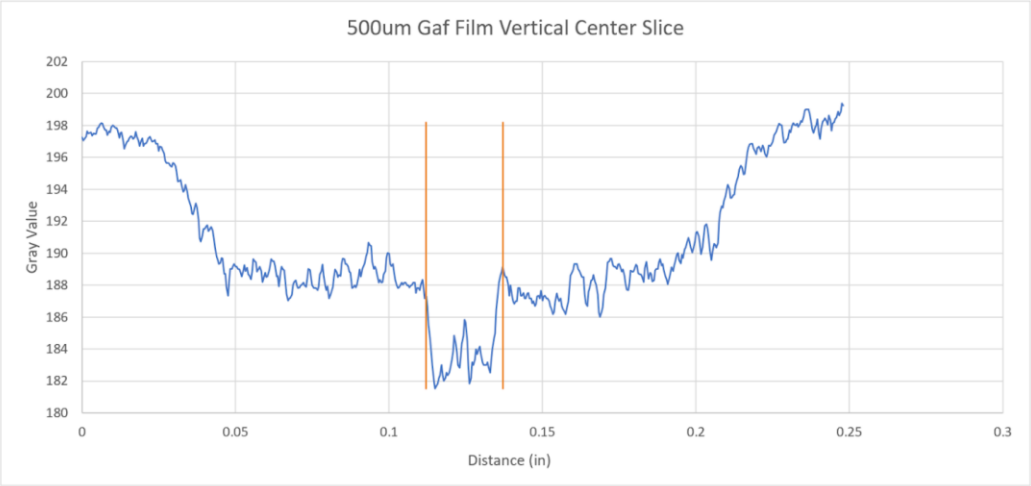

Figure 4.17: Copper 500µm Raw Data Vertical Slice

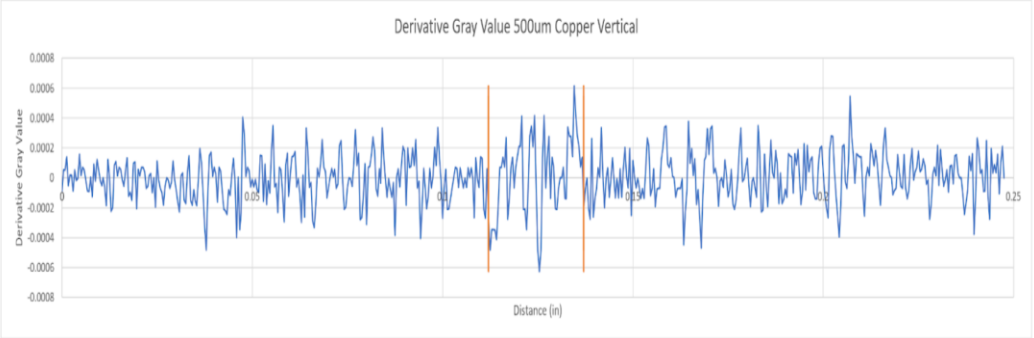

Figure 4.18: Copper 500µm Derivative Data Vertical Slice

Observation of the Gaf film in figure 4.14, shows a lightly dosed large circle with a distinct darker circle in the middle. This suggests that the thickness of the Copper material was not thick enough to completely stop the beam. According to the Suess Software package, the minimum thickness required for copper to fully stop the beam is 49.6µm. The Copper apertures used in this research had a thickness of 25µm, further

validating that the aperture did not fully stop the beam. The reason for procuring this thinner material and proposed solution is covered in section 4.4.

The horizontal slice measurement was measured to be 560.9082µm, and the vertical slice was measured to be 635µm, producing an average dosed diameter of 597.95µm. It is speculated that the main reason why the dosed diameter is larger than the physical hole diameter is because of timed constrained testing times. There was a maximum of 30 minutes allotted for us to run a test, as we were essentially borrowing beam time from Texas Instruments. This led to setting up the next test run as fast as possible, which introduced alignment errors of the film. If the film is not aligned correctly, this will result in different horizontal and vertical measurements. Additionally, it was difficult to identify the starting and ending points of the dosed diameter, due to noisy data. Regardless, the test shows that the aperture can effectively reduce the beam to desired diameters.

The second analysis is the 500µm diameter fiber laser Aluminum aperture. The same figure format is followed.

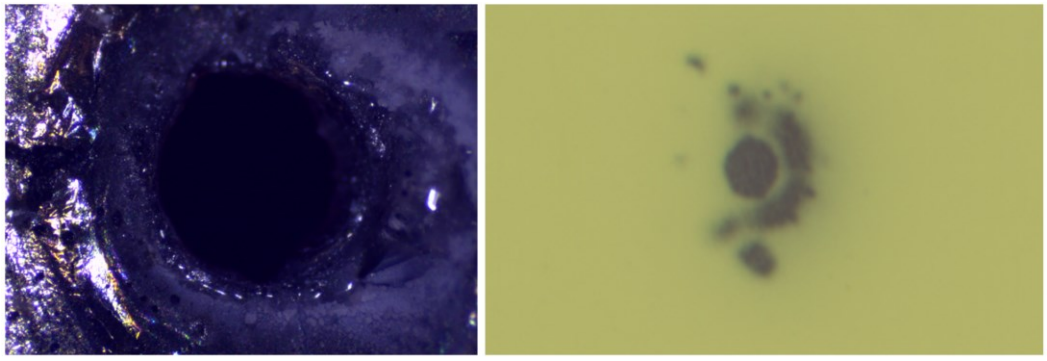

Figure 4.19: Aluminum Fiber Laser 500µm Gaf Film Image Scan

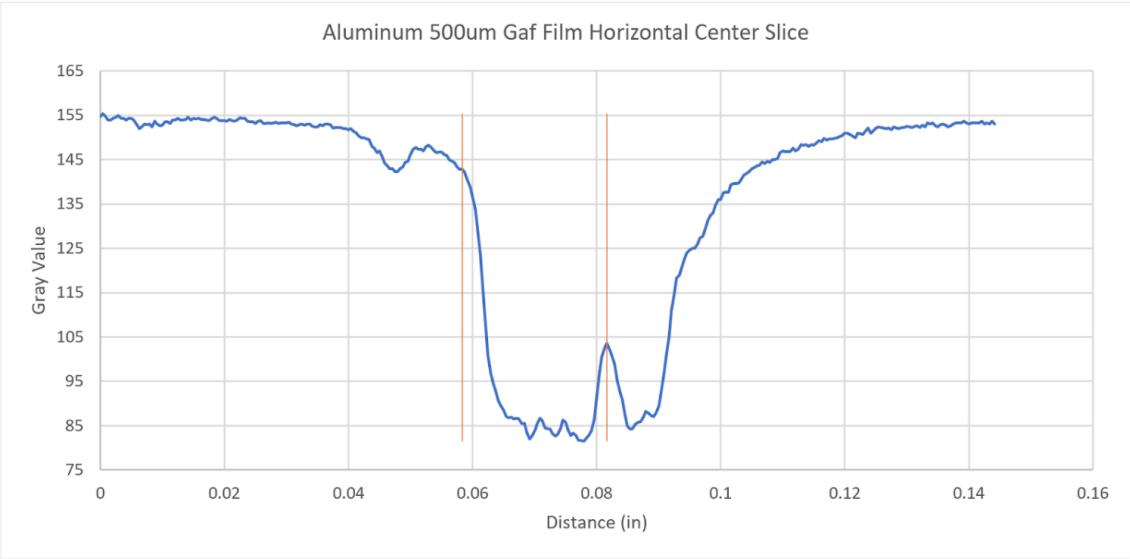

Figure 4.20: Aluminum Fiber Laser 500µm Raw Data Horizontal Slice

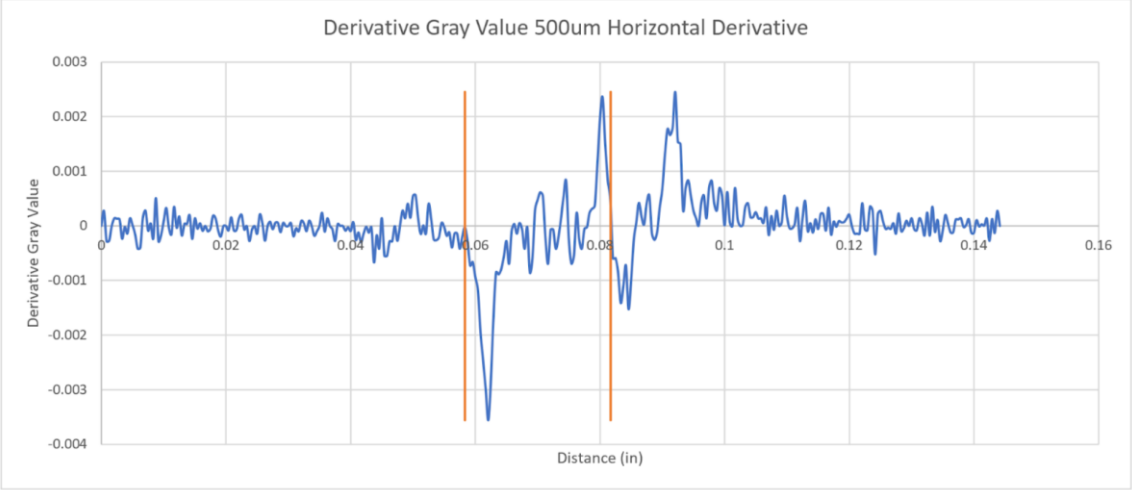

Figure 4.21: Aluminum Fiber Laser 500µm Derivative Data Horizontal Slice

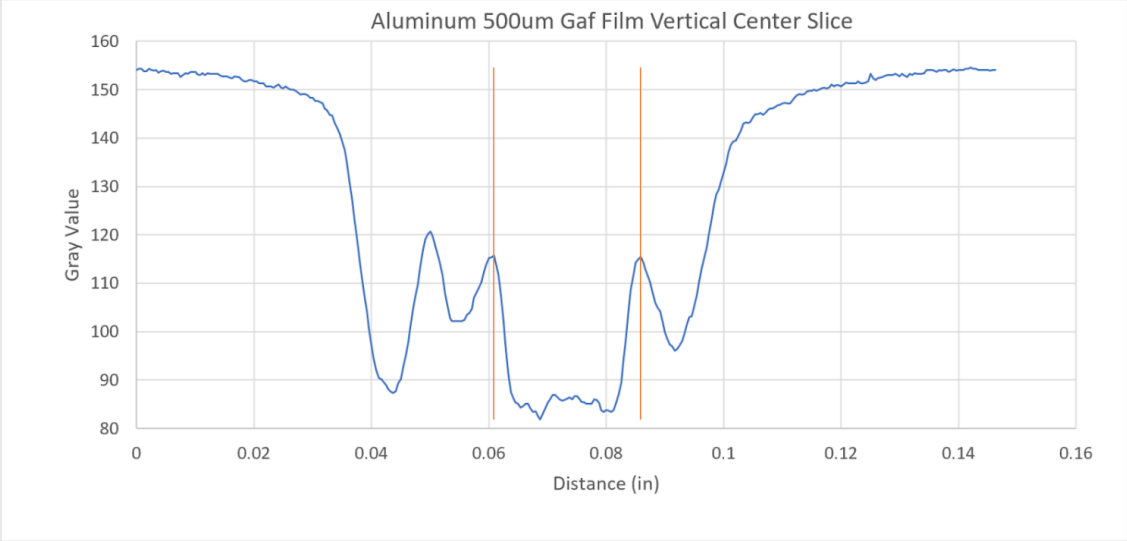

Figure 4.22: Aluminum Fiber Laser 500µm Raw Data Vertical Slice

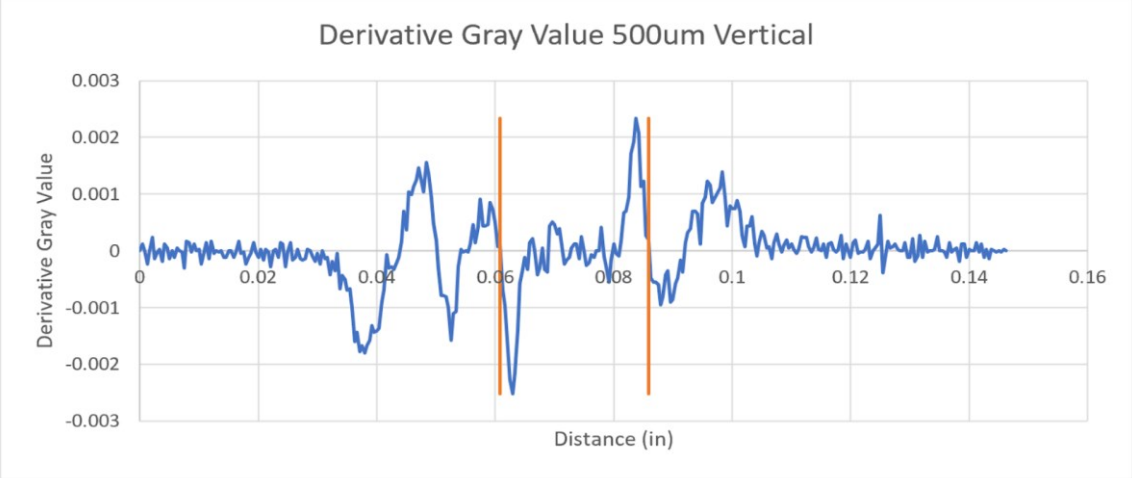

Figure 4.23: Aluminum Fiber Laser 500µm Derivative Data Vertical Slice

Observing the Gaf film image scan in Figure (4.19), there is a dominant center circle surrounded by undesired dosed sections. The undesired sections directly correlate to the melted edges of the hole. The thickness of the melted sections falls below the

required minimum thickness to stop the beam and results in the beam penetrating through the material shield and affecting the dosed diameter. This further proves that high-quality edge characteristics are required for a high-quality dosed diameter. The derivative transformation of the raw data was effective enough to determine a clear starting and ending point of the desired diameter, resulting in 592.68µm horizontal measurement and 635µm vertical measurement. This results in an average dosed diameter of 613.84µm.

The third analysis is the 1000µm diameter fiber laser Aluminum aperture. The same figure format is followed as above.

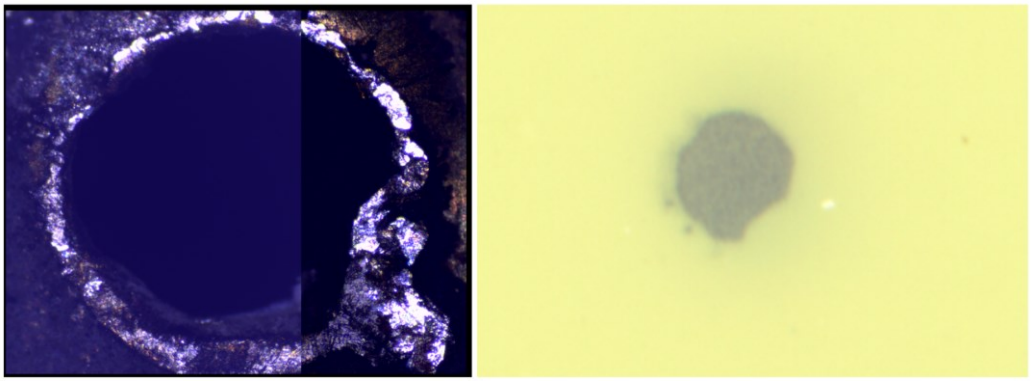

Figure 4.24: Aluminum Fiber Laser 1000µm Gaf Film Image Scan

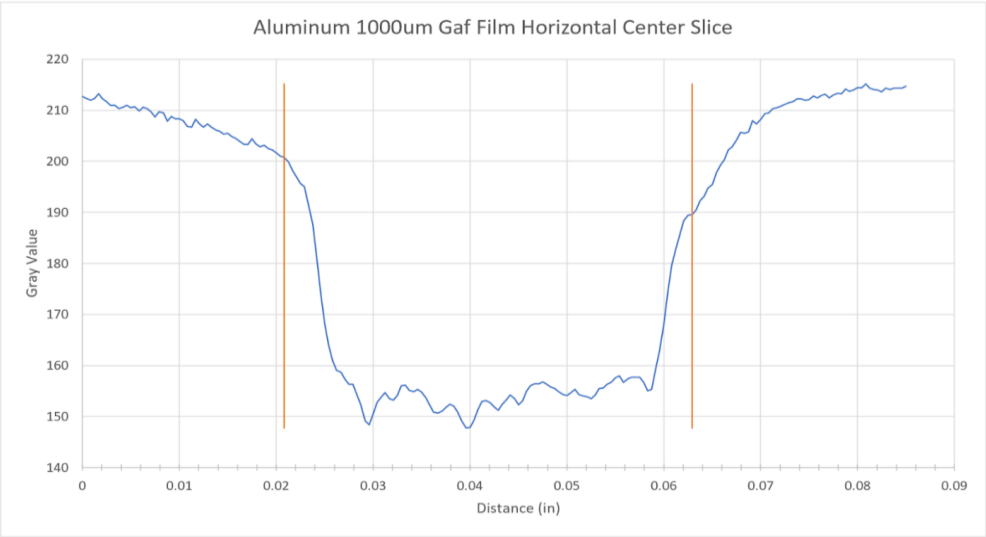

Figure 4.25: Aluminum Fiber Laser 1000µm Raw Data Horizontal Slice

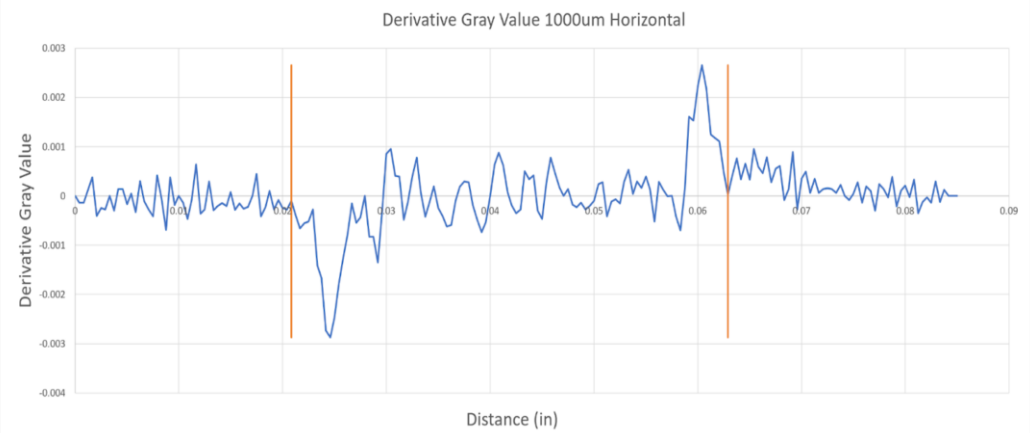

Figure 4.26: Aluminum Fiber Laser 1000µm Derivative Data Horizontal Slice

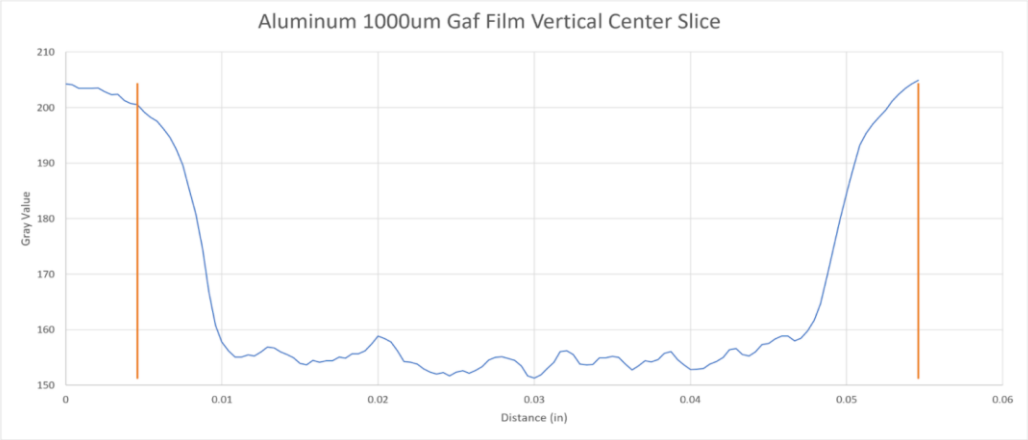

Figure 4.27: Aluminum Fiber Laser 1000µm Raw Data Vertical Slice

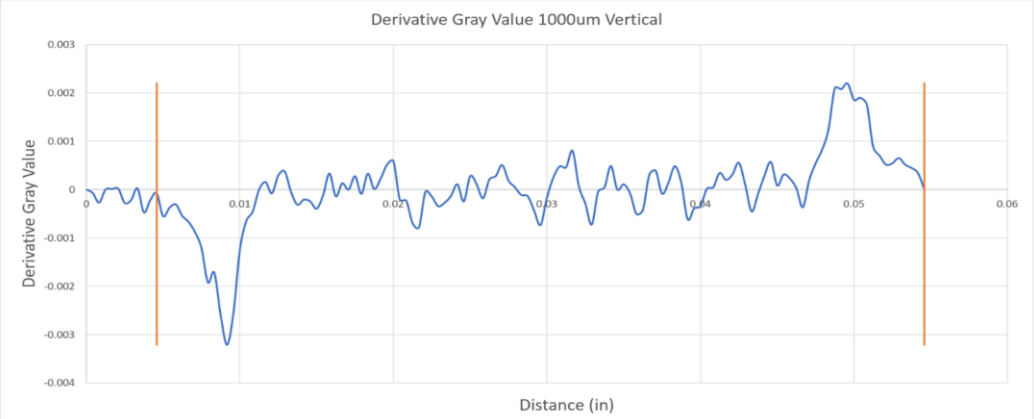

Figure 4.28: Aluminum Fiber Laser 1000µm Derivative Data Vertical Slice

The Gaf film scan in Figure (4.24) shows how the edge defect of the hole directly affects the reduced beam quality. Again, this provides additional evidence that a high-quality edge is required for a circular reduced beam. The horizontal slice measurement of the dosed diameter for this aperture is 1068.91µm and vertical measurement of 1270µm. The edge defect is taken into account for measurement resulting in a large difference between measurements. The average dosed diameter is 1169.45µm.

The final dosed diameter analysis is the 700µm diameter razor blade Aluminum aperture serving as our baseline test. The same figure format is followed as above.

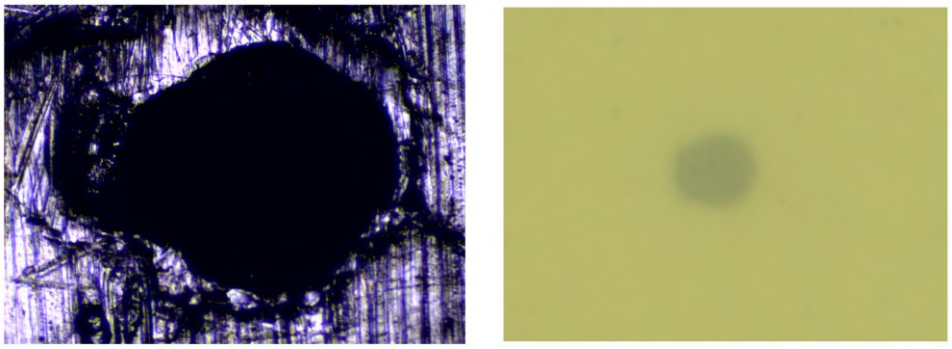

Figure 4.29: Aluminum Razor Blade 700µm Gaf Film Image Scan

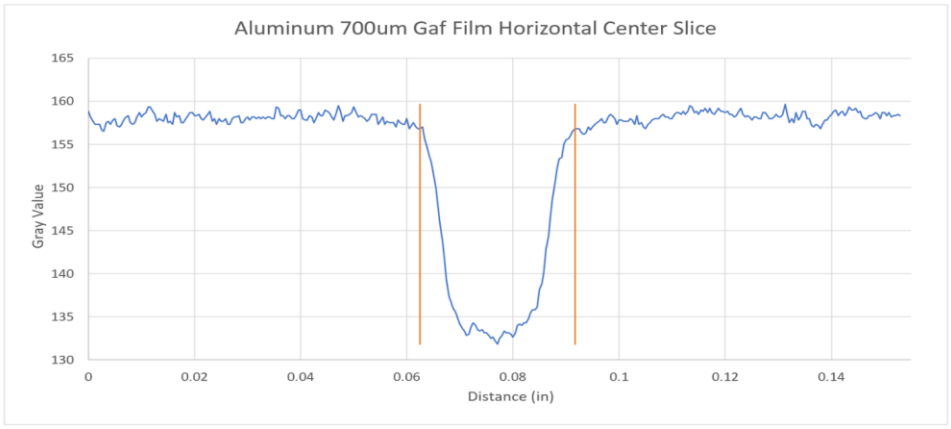

Figure 4.30: Aluminum Razor Blade 700µm Raw Data Horizontal Slice

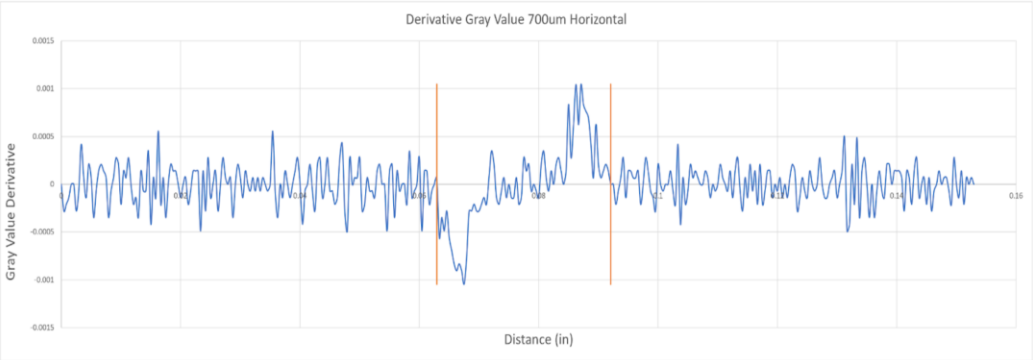

Figure 4.31: Aluminum Razor Blade 700µm Derivative Data Horizontal Slice

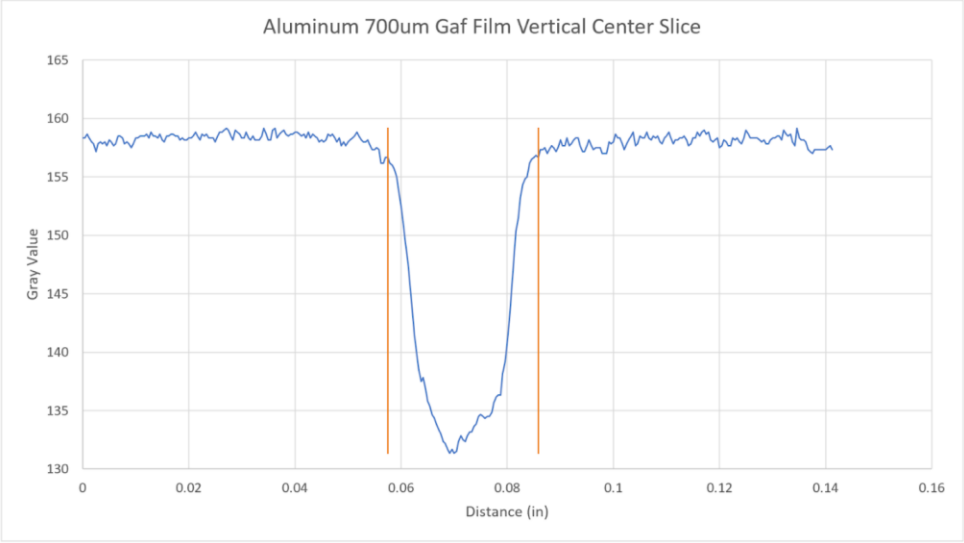

Figure 4.32: Aluminum Razor Blade 700µm Raw Data Vertical Slice

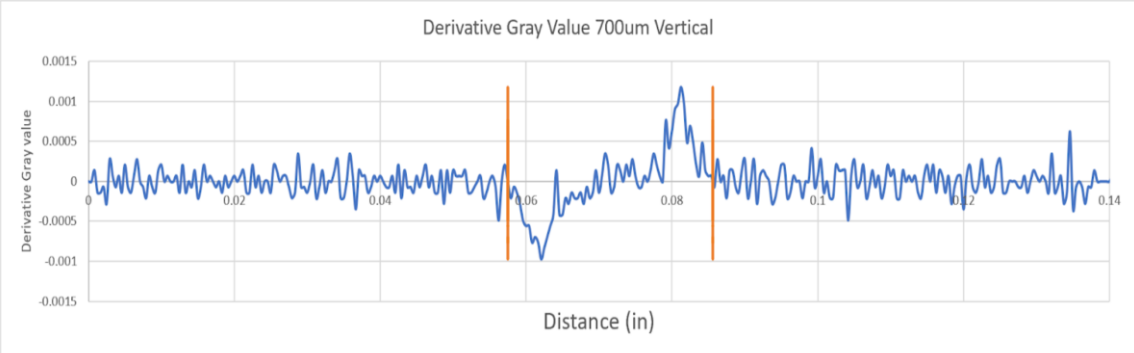

Figure 4.33: Aluminum Razor Blade 700µm Derivative Data Vertical Slice

The same edge defect phenomenon can also be seen in the Gaf film image scan. The large defect directly affects the quality of the reduced beam. The horizontal measurement is 740.81µm, and the vertical measurement is 713.74µm. The average dosed diameter is 727.27µm.

4.3 Gaf Film Diffusion Measurement

The purpose of the Gaf film reduced beam diffusion test is to measure how much the reduced diameter beam spreads over a total 27mm air gap. The reduced diameter beam is never expected to propagate further than 4mm until it encounters the DUT surface. The large air gap was primarily chosen to exaggerate beam diffusion and to reveal any underlying issues that cannot be identified with a smaller air gap.

As discussed previously, there are two distances of Gaf film to aperture separation where measurements are taken: 2mm and 29mm. The previously recorded dosed diameter will serve as measurements for 2mm. This section will display the results for 29mm separation using both fiber laser Aluminum apertures as beam reduction devices. The same techniques are used to measure horizontal and vertical distances; therefore, the figure format will be the same as before.

The first sample being analyzed is the 1000µm diameter fiber laser Aluminum aperture with a Gaf film separation distance of 29mm.

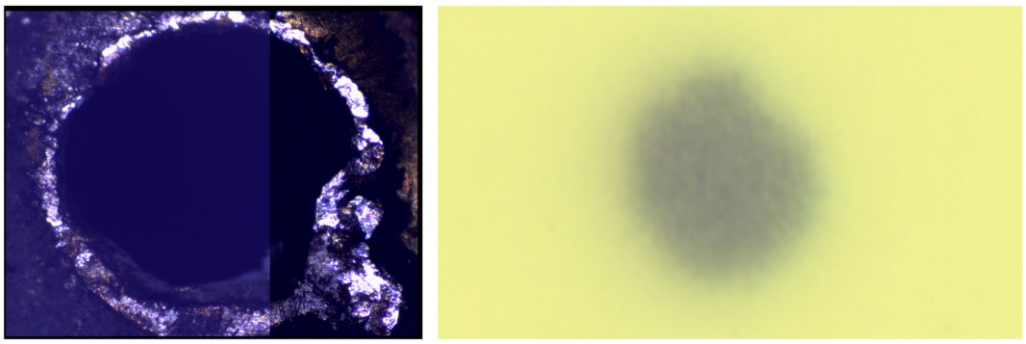

Figure 4.34: Aluminum Fiber Laser 1000µm Gaf Film Image Scan 29mm

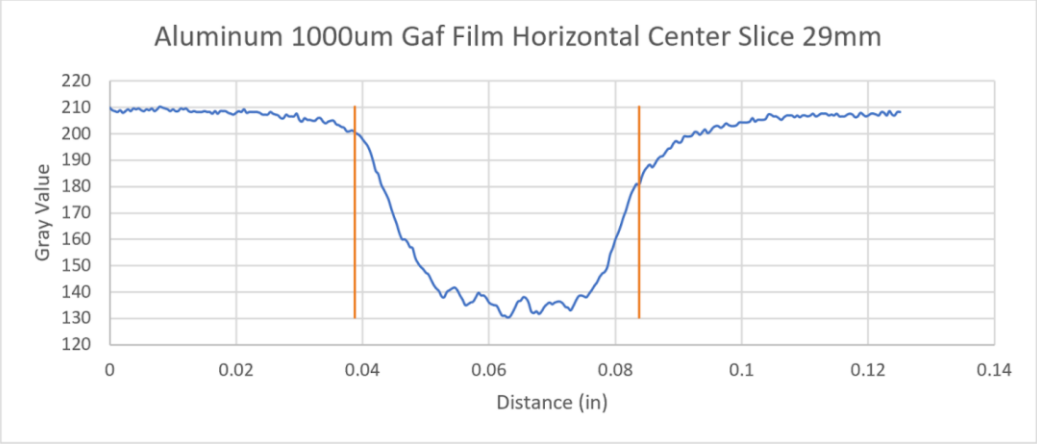

Figure 4.35: Aluminum Fiber Laser 1000µm Raw Data Horizontal Slice 29mm

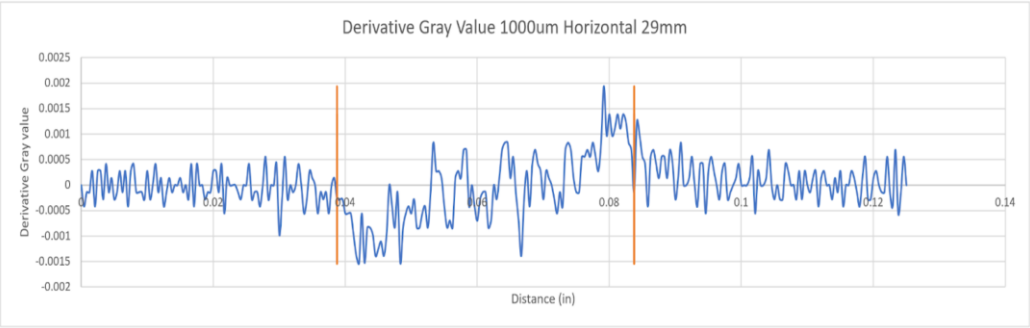

Figure 4.36: Aluminum Fiber Laser 1000µm Derivative Data Horizontal 29mm

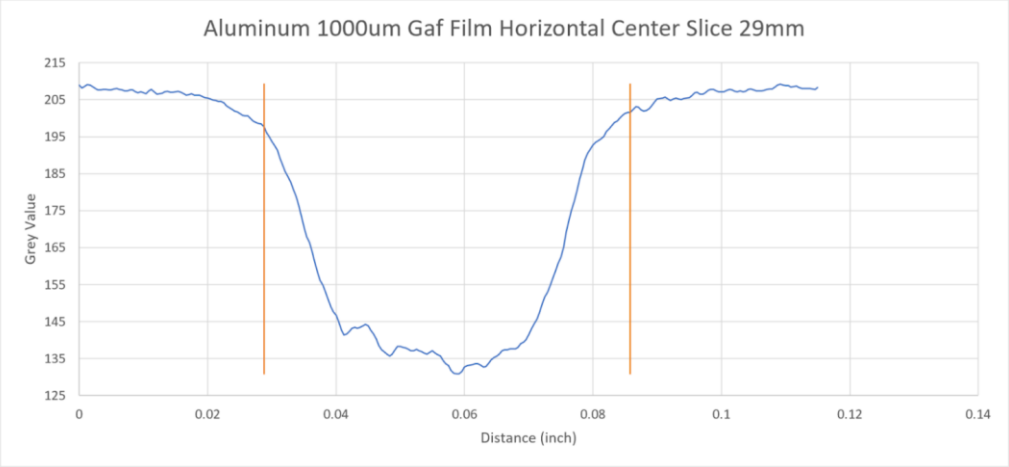

Figure 4.37: Aluminum Fiber Laser 1000µm Raw Data Vertical Slice 29mm

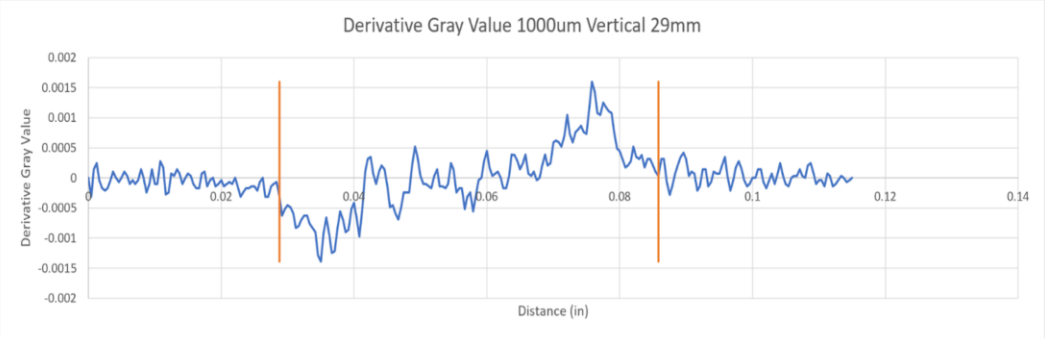

Figure 4.38: Aluminum Fiber Laser 1000µm Derivative Data Vertical Slice 29mm

Observing the Gaf film, the dosed diameter gray imprint is not as defined as seen with samples at 2mm. In this case, the gray imprint gradually becomes darker towards the center. This suggests that there is in fact reduced beam diffusion, effectively lowering the cross-sectional flux of heavy ions at far away distances compared to close distances. This is also another driving factor for the derivative transformation so that it is easier to identify where the start and endpoints should be selected.

The horizontal distance was measured to be 1206.5µm at 29mm and the vertical distance was measured to be 1449.9µm at 29mm. Overall reduced beam diffusion was calculated by finding the difference between the 2mm measurements and the 29mm measurements, reducing the result to reflect diffusion per millimeter, and then taking the average diffusion of the horizontal and vertical results. For this analysis, the horizontal diffusion is 5.09µm per 1mm, and vertical diffusion is 6.66µm per 1mm. The average reduced beam diffusion resulted in 5.875µm per 1mm.

The second sample being analyzed is the 500µm diameter fiber laser Aluminum aperture with a Gaf film separation distance of 29mm.

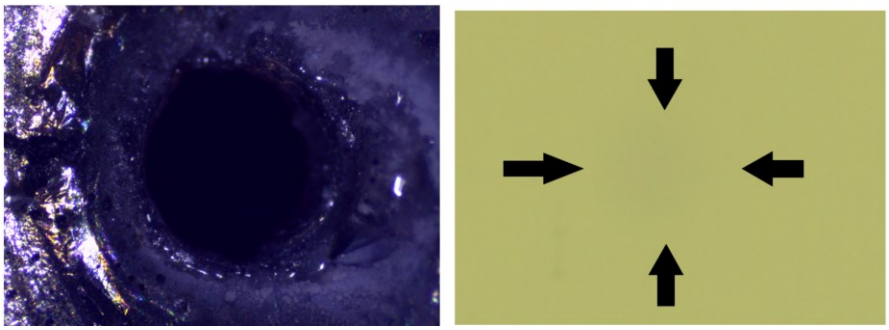

Figure 4.39: Aluminum Fiber Laser 500µm Gaf Film Image Scan 29mm

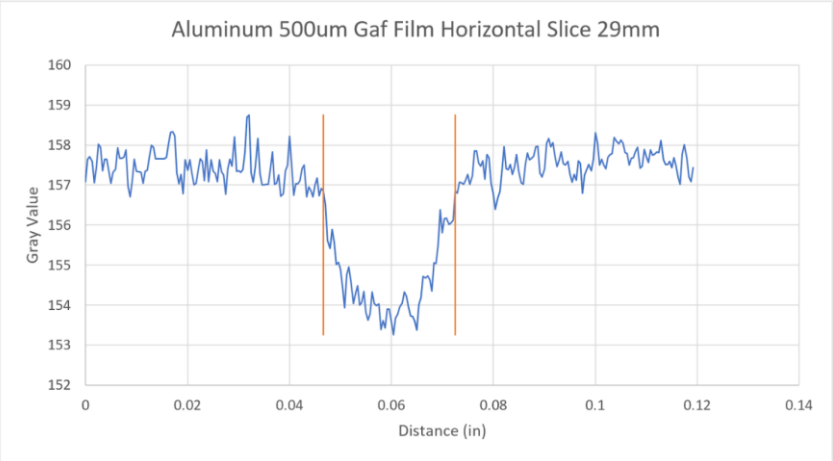

Figure 4.40: Aluminum Fiber Laser 500µm Raw Data Horizontal Slice 29mm

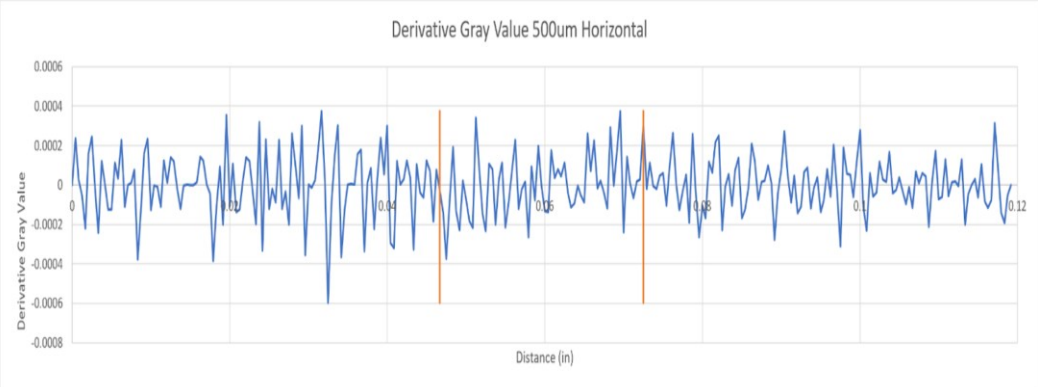

Figure 4.41: Aluminum Fiber Laser 500µm Derivative Data Horizontal Slice 29mm

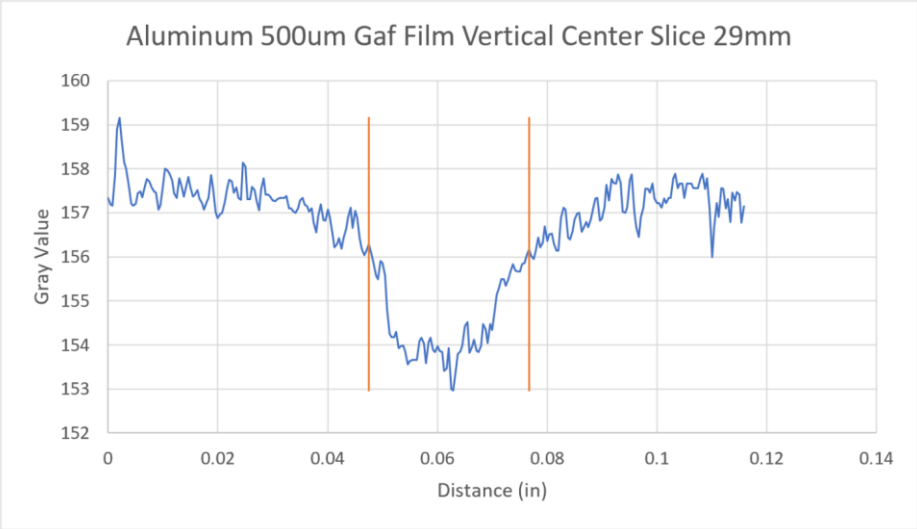

Figure 4.42: Aluminum Fiber Laser 500µm Raw Data Vertical Slice 29mm

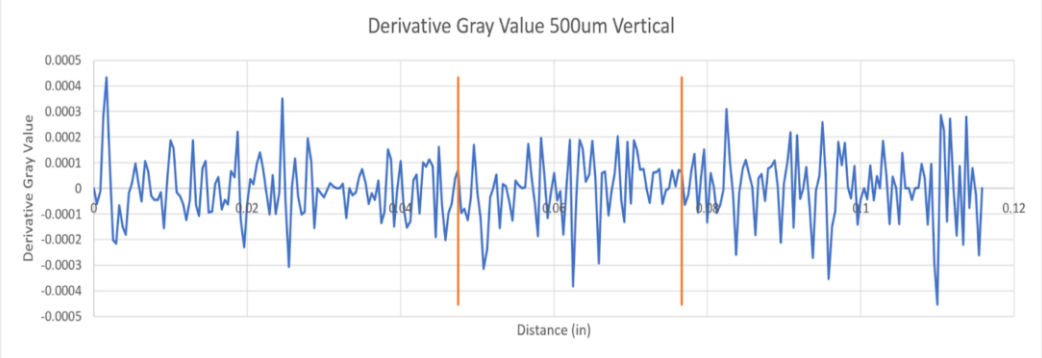

Figure 4.43: Aluminum Fiber Laser 500µm Derivative Data Vertical Slice 29mm

As shown in Figure 4.39, it is difficult to visually see any gray imprint in this document, as the beam had just enough energy to make an effect on the film. Viewing the film in person, I was able to visually see where the imprint was located, and ImageJ was able to produce sufficient data for analysis. The horizontal distance was measured to be 656.1582µm, and the vertical distance was measured to be 740.8418µm. This reduces

to 2.35 per 1mm horizontally and 3.92µm per 1mm vertically, resulting in an average reduced beam diffusion of 3.135µm per 1mm.

Assuming that alignment error is taken into effect, we take the average diffusion between the two samples to generate an idea of overall reduced beam diffusion across multiple samples to be 4.505µm per 1mm.

4.4 Key Issues Discovered and Solutions

As discussed previously, the Lenox Laser Copper apertures did not fully stop the undesired sections of the beam. The minimum thickness required for copper to stop the beam is 49.6µm. The high-power apertures have a thickness of 25µm, such that the beam penetrated through the entire aperture material and interacted with the Gaf film.

The cyclotron has the ability to reduce the beam strength by use of an Aluminum foil degrader that is either manually set by the user or by the software after inputting the desired ion energy at the surface of the DUT. To be shielded, Texas Instruments requires a DUT penetration value of no more than 50µm. During testing sessions, the 15 MeV/u Holmium beam with no degrader and a 40mm air gap layer setting has an estimated DUT penetration range of 95.8µm as shown in figure 4.44. This is well above the maximum penetration value.

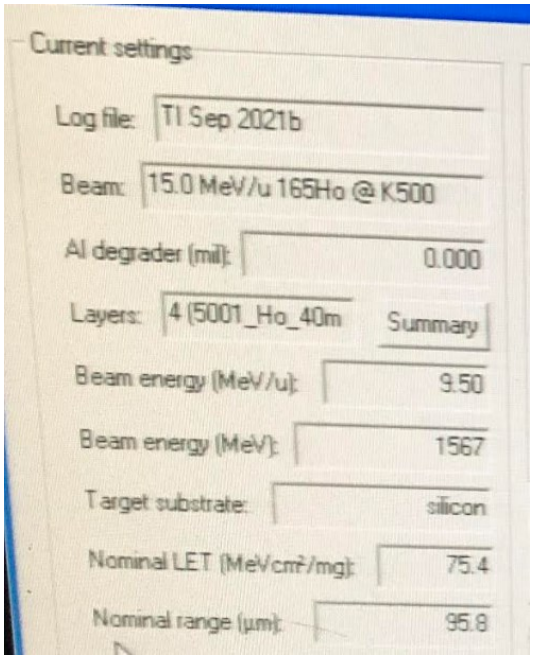

Figure 4.44: Texas Instruments Standard Test Settings

The overall goal of this solution is to adjust the beam degrader foil to reduce the beam energy where the 25µm thick copper aperture effectively stops the undesired sections of the beam. By changing the layer settings to reflect the Copper aperture configuration, shown in figure 4.45, we can adjust the desired beam energy at the DUT surface to 0.001 MeV/u, resulting in 0µm of DUT penetration. The Suess software will automatically adjust the beam degrader foil to reflect this value. It is important to note that these calculations are heavily dependent on the selected layer settings and current beam configuration. Once the degrader is moved into position, the layer settings is then changed to the standard 40mm air gap configuration shown in figure 4.46, and a new DUT penetration range is calculated. This will reflect the beam that is traveling through

the micrometer scale hole of the aperture. The new DUT penetration range is estimated to be 63.2µm (figure 4.47) which is acceptable for Texas Instruments.

silicon	ROT	0	um
air gas	FIX	2	mm
copper	FIX	25	um
air gas	FIX	38	mm
aramica	FIX	25.4	um

Figure 4.45: Copper Aperture Layer Settings

silicon	ROT	0	um
air gas	FIX	40000	um
aramica	FIX	25.4	um

Figure 4.46: 40mm Air Gap Layer Settings

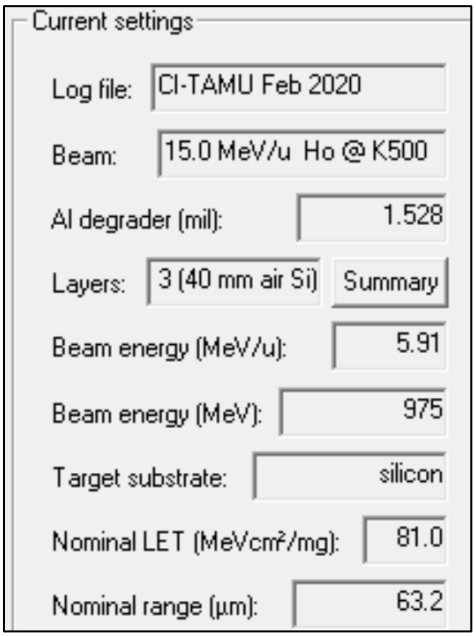

Figure 4.47: Tuned Degrader DUT Penetration Value

5. CONCLUSIONS

5.1 Summary

Single Event Effects testing is an important part of designing effective radiation-hardened semiconductor devices for space environments. Texas Instruments needed a system capable of isolating specific transistor groups, which requires reducing the heavy ion beam to micrometer level diameters. By using the combination of micro-machined apertures and a high precision alignment system, test engineers can reduce the time and labor of isolating the transistor groups and perform test runs at a higher rate. This paper identifies the background material, methods, results, and key issues of reducing the heavy ion beam to a high-quality micrometer level diameter beam that can be aligned to specifically target these transistor groups. This proposed method shows large promise in the application of this system to enhance Texas Instruments' ability to identify weak sections within their devices and design high-quality radiation-hardened semiconductor devices for space applications.

5.2 Future Work

Fine-tuning the cyclotron beam degrader system can be avoided by procuring 75µm thick Copper apertures from Lenox Laser.

6. REFENCES

[1] M. F. A. Ziata, "Radioactivity (Introduction and History)," 2007.

[2] O. Firsov, "A qualitative interpretation of the mean electron excitation energy in atomic collisions," Zhur. Eksptl'. i Teoret. Fiz., vol. 36, 1959.

[3] J. G. Drobny, Ionizing radiation and polymers: principles, technology, and applications. William Andrew, 2012.

[4] A. Mozumder, Fundamentals of radiation chemistry. Elsevier, 1999.

[5] H. Kozima, The Science of the Cold Fusion Phenomenon: In Search of the Physics and Chemistry Behind Complex Experimental Data Sets. Elsevier, 2006.

[6] J. E. Turner, "Interaction of ionizing radiation with matter," Health physics, vol. 88, no. 6, pp. 520-544, 2005.

[7] G. Venugopal, S. Saini, and S.-J. Kim, "Focused Ion Beam Based Three-Dimensional Nano-Machining," Micromachining Techniques for Fabrication of Micro and Nano Structures, pp. 1-16, 2012.

[8] X. Wang, G. Y. Mak, and H. W. Choi, "Laser micromachining and micro-patterning with a nanosecond UV laser," Micromachining Techniques for Fabrication of Micro and Nano Structures, vol. 1, pp. 85-109, 2012.

[9] B. Breidenstein, T. Mörke, R. Hockauf, J. Jörn Ostermann, and B. Spitschan, "2. Sensors, data storage and communication technologies. In book “Cyber-Physical and Intelligent Systems in Manufacturing and Life Cycle. Genetics and Intelligence-Keys to Industry 4.0”," ed: Academic Press, 2017.

[10] E. P. DeGarmo, J. T. Black, R. A. Kohser, and B. E. Klamecki, Materials and process in manufacturing. Prentice Hall Upper Saddle River, 1997.

[11] Krystian L. Wlodarczyk, Adam Brunton, Phil Rumsby, and Duncan P. Hand, Picosecond laser cutting and drilling of thin flex glass. Optics and Lasers in Engineering,

Volume 78, 2016, Pages 64-74